RESEARCH ARTICLE
PLANETARY SCIENCE

*Earth and Planetary Physics*
*2*: 22–39, 2018
doi: 10.26464/epp2018003

# Efficient metal emissions in the upper atmospheres of close-in exoplanets

**Lei Liu, and Feng Tian***

Department of Earth System Science, Tsinghua University, Beijing 100084, China

**Abstract:** Atmospheric escape is a key process controlling the long term evolution of planets. Radiative cooling competes for energy against atmospheric escape in planetary upper atmospheres. In this work, we use a population balance method and a Monte Carlo model to calculate the previously ignored emissions of metals (C, N, O and their ions) and compare them with radiative recombination of H II and Ly-α emission of H I, which are the most efficient cooling mechanisms currently recognized in the upper atmospheres of hot Jupiters. The results show that the emissions of C, N, O and their ions are strong non-linear functions of environmental parameters (temperature, density, etc.) and are likely to be efficient cooling mechanisms in the upper atmospheres of close-in exoplanets.

**Keywords:** exoplanet; upper atmosphere; emission

**Citation:** Liu L., and Tian F. (2018). Efficient metal emissions in the upper atmospheres of close-in exoplanets. *Earth Planet. Phys.*, *2*, 22–39. http://doi.org/10.26464/epp2018003

## 1. Introduction

Radiative cooling is a key consideration in calculating the heating efficiencies in planetary upper atmospheres (Tian F, 2015). Heating efficiency describes the fraction of absorbed XUV photons converted to kinetic energy. Radiative recombination of H II and Ly-$\alpha$ emission of H I are the most efficient cooling mechanisms recognized today for the upper atmosphere of close-in exoplanets (Murray-Clay et al., 2009; Koskinen et al., 2013a). Although the column-integrated emission of $H_3^+$ is larger than these emissions (Shaikhislamov et al., 2014; Yelle, 2004), it is insignificant from the perspective of atmosphere loss because of the low abundance of $H_3^+$ in the middle and upper parts of planetary thermospheres. Most numerical models for H-dominant planetary upper atmospheres (Yelle, 2004; Tian F et al., 2005; Murray-Clay et al., 2009; Koskinen et al., 2013a, b ) adopt heating efficiencies of ~10%, which is consistent with empirical analysis of exoplanet observations (Lopez et al., 2012) and detailed numerical models for pure hydrogen upper atmospheres (Shematovich et al., 2014). With this efficiency, rocky planets under strong stellar wind and XUV radiation could rapidly lose their volatiles (Tian F, 2015; Massol et al., 2016).

C and O have been observed in the extended H envelopes of hot Jupiters (Vidal-Madjar et al., 2004; Linsky et al., 2010) and are expected to be abundant in the upper atmospheres of strongly XUV-irradiated rocky planets (Tian F, 2009, 2015; Tian F et al., 2008a, b, 2009). The O/H ratio in the upper atmospheres of planets experiencing rapid water loss should be ~0.5 (Tian F, 2015; Massol et al., 2016). These species and other metals could also be delivered to planets by interplanetary dust particles. Besides, oxygen ion escape could be as important as H escape in water loss under strong XUV radiation (Airapetian et al., 2017). But the radiative effects of metals have been largely ignored in previous studies.

In this work, we developed a population balance model and a Monte Carlo model to calculate the population distributions and emissions of C, N, O (and their ions) by considering collisional excitation, collisional deexcitation, and spontaneous emission, based on fundamental data in the literature. We found that metal emissions appear to be important cooling mechanisms for typical close-in exoplanets and suggest that future numerical models of the upper atmospheres of such planets should include metal emissions.

## 2. Methods

Tables 1 and 2 show the energy states and corresponding Einstein coefficients ($s^{-1}$) included in our model. Between 8 and 14 energy states are considered to ensure that metal emissions increase by no more than 3% when additional excited states are considered.

### 2.1 Population Balance Model

The population balance model solves a series of species-relevant equilibrium equations for C, N, O, and their ions. For the number density of any metal species at energy state $j$ ($N_j$), the following equation can be written (all terms with the unit of $cm^{-3}\cdot s^{-1}$):

$$N_j\sum_{i=1}^{j-1}A_{ji}+N_j\sum_{i=1}^{j-1}C_{ji}+N_j\sum_{k>j}C_{jk}=\sum_{k>j}N_kA_{kj}+\sum_{k>j}N_kC_{kj}+\sum_{i=1}^{j-1}N_iC_{ij}, \quad (1)$$

Correspondence to: F. Tian, tianfengco@tsinghua.edu.cn
Received 13 SEP 2017; Accepted 29 DEC 2017.
Accepted article online 26 JAN 2018.

**Table 1.** Energy states of metals considered in this work

| *n* | Parameters | C I | C II | N I | N II | O I | O II |
|---|---|---|---|---|---|---|---|
| 1 | Energy (eV) | 0 | 0 | 0 | 0 | 0 | 0 |
| | Degeneracy | 1 | 2 | 4 | 1 | 5 | 4 |
| | Configuration | $^3P_0$ | $^2P^o_{1/2}$ | $^4S^o_{3/2}$ | $^3P_0$ | $^3P_2$ | $^4S^o_{3/2}$ |
| 2 | Energy (eV) | 0.0020 | 0.0079 | 2.38353 | 0.0060 | 0.01962 | 3.324 |
| | Degeneracy | 3 | 4 | 6 | 3 | 3 | 6 |
| | Configuration | $^3P_1$ | $^2P^o_{3/2}$ | $^2D^o_{5/2}$ | $^3P_1$ | $^3P_1$ | $^2D^o_{5/2}$ |
| 3 | Energy (eV) | 0.0054 | 5.3317 | 2.38461 | 0.0162 | 0.02814 | 3.327 |
| | Degeneracy | 5 | 2 | 4 | 5 | 1 | 4 |
| | Configuration | $^3P_2$ | $^4P_{1/2}$ | $^2D^o_{3/2}$ | $^3P_2$ | $^3P_0$ | $^2D^o_{3/2}$ |
| 4 | Energy (eV) | 1.2637 | 5.3345 | 3.57557 | 1.8990 | 1.96736 | 5.017 |
| | Degeneracy | 5 | 4 | 2 | 5 | 5 | 4 |
| | Configuration | $^1D_2$ | $^4P_{3/2}$ | $^2P^o_{1/2}$ | $^1D_2$ | $^1D_2$ | $^2P^o_{3/2}$ |
| 5 | Energy (eV) | 2.6840 | 5.3380 | 3.57562 | 4.0529 | 4.18975 | 5.018 |
| | Degeneracy | 1 | 6 | 4 | 1 | 1 | 2 |
| | Configuration | $^1S_0$ | $^4P_{5/2}$ | $^2P^o_{3/2}$ | $^1S_0$ | $^1S_0$ | $^2P^o_{1/2}$ |
| 6 | Energy (eV) | 4.1826 | 9.2901 | 10.32591 | 5.8006 | 9.14609 | 14.858 |
| | Degeneracy | 5 | 6 | 2 | 5 | 5 | 6 |
| | Configuration | $^5S^o_2$ | $^2D_{5/2}$ | $^4P_{1/2}$ | $^5S^o_2$ | $^5S^o_2$ | $^4P_{5/2}$ |
| 7 | Energy (eV) | 7.4804 | 9.2905 | 10.33009 | 11.4360 | 9.52136 | 14.878 |
| | Degeneracy | 1 | 4 | 4 | 7 | 3 | 4 |
| | Configuration | $^3P^o_0$ | $^2D_{3/2}$ | $^4P_{3/2}$ | $^3D^o_3$ | $^3S^o_1$ | $^4P_{3/2}$ |
| 8 | Energy (eV) | 7.4828 | 11.9637 | 10.33590 | 11.4376 | 10.74023 | 14.888 |
| | Degeneracy | 3 | 2 | 6 | 5 | 3 | 2 |
| | Configuration | $^3P^o_1$ | $^2S_{1/2}$ | $^4P_{5/2}$ | $^3D^o_2$ | $^5P_1$ | $^4P_{1/2}$ |
| 9 | Energy (eV) | 7.4878 | | 10.67967 | 11.4378 | 10.74048 | |
| | Degeneracy | 5 | | 2 | 3 | 5 | |
| | Configuration | $^3P^o_2$ | | $^2P_{1/2}$ | $^3D^o_1$ | $^5P_2$ | |
| 10 | Energy (eV) | 7.6848 | | 10.68998 | 13.5411 | 10.74093 | |
| | Degeneracy | 3 | | 4 | 3 | 7 | |
| | Configuration | $^1P^o_1$ | | $^2P_{3/2}$ | $^3P^o_1$ | $^5P_3$ | |
| 11 | Energy (eV) | 7.9458 | | 10.92391 | 13.5413 | 10.98879 | |
| | Degeneracy | 7 | | 6 | 5 | 3 | |
| | Configuration | $^3D^o_3$ | | $^4P_{5/2}$ | $^3P^o_2$ | $^3P_1$ | |
| 12 | Energy (eV) | 7.9461 | | 10.92935 | 13.5420 | 10.98886 | |
| | Degeneracy | 3 | | 4 | 1 | 5 | |
| | Configuration | $^3D^o_1$ | | $^4P_{3/2}$ | $^3P^o_0$ | $^3P_2$ | |
| 13 | Energy (eV) | 7.9463 | | 10.93176 | | 10.98888 | |
| | Degeneracy | 5 | | 2 | | 1 | |
| | Configuration | $^3D^o_2$ | | $^4P_{1/2}$ | | $^3P_0$ | |
| 14 | Energy (eV) | | | 11.60263 | | | |
| | Degeneracy | | | 2 | | | |
| | Configuration | | | $^2S^o_{1/2}$ | | | |

**Table 2.** Einstein coefficients ($s^{-1}$) used in this work

3(–1) represents $3\times10^{-1}$

| Transitions | C I | C II | N I | N II | O I | O II |
|---|---|---|---|---|---|---|
| $A_{21}$ | 7.93 (–8) | 2.29 (–6) | 6.59 (–6) | 2.08 (–6) | 8.91 (–5) | 2.86 (–5) |
| $A_{31}$ | 0 | 5.99 (1) | 1.60 (–5) | 1.12 (–12) | 1.34 (–10) | 1.59 (–4) |
| $A_{32}$ | 2.65 (–7) | 6.78 (1) | 1.07 (–8) | 7.46 (–6) | 1.75 (–5) | 1.30 (–7) |
| $A_{41}$ | 0 | 1.40 | 2.60 (–3) | 5.25 (–7) | 5.63 (–3) | 5.22 (–2) |
| $A_{42}$ | 7.28 (–5) | 8.49 | 3.45 (–2) | 9.84 (–4) | 1.82 (–3) | 9.07 (–2) |
| $A_{43}$ | 2.17 (–4) | 0 | 5.20 (–2) | 2.91 (–3) | 8.60 (–7) | 3.85 (–2) |
| $A_{51}$ | 0 | 0 | 6.50 (–3) | 0 | 2.42 (–4) | 2.12 (–2) |
| $A_{52}$ | 2.32 (–3) | 4.43 (1) | 6.00 (–2) | 3.18 (–2) | 7.54 (–2) | 5.19 (–2) |
| $A_{53}$ | 0 | 0 | 2.56 (–2) | 1.55 (–4) | 0 | 7.74 (–2) |
| $A_{54}$ | 5.99 (–1) | 0 | 0 | 1.14 | 1.26 | 1.41 (–10) |
| $A_{61}$ | 0 | 0 | 4.00 (8) | 0 | 4.20 (3) | 8.61 (8) |
| $A_{62}$ | 8.60 | 2.88 (8) | 0 | 5.15 (1) | 1.36 (3) | 0 |
| $A_{63}$ | 2.10 (1) | 0 | 0 | 1.27 (2) | 0 | 0 |
| $A_{64}$ | 0 | 0 | 0 | 9.33 (–4) | 5.32 (–3) | 0 |
| $A_{65}$ | 0 | 0 | 0 | 0 | 0 | 0 |
| $A_{71}$ | 0 | 2.41 (8) | 4.03 (8) | 0 | 3.41 (8) | 8.65 (8) |
| $A_{72}$ | 3.47 (8) | 4.76 (7) | 0 | 0 | 2.03 (8) | 0 |
| $A_{73}$ | 0 | 0 | 0 | 3.72 (8) | 6.76 (7) | 0 |
| $A_{74}$ | 0 | 0 | 0 | 4.14 (3) | 1.83 (3) | 0 |
| $A_{75}$ | 0 | 0 | 0 | 0 | 4.61 | 0 |
| $A_{76}$ | 0 | 0 | 0 | 0 | 0 | 0 |
| $A_{81}$ | 1.16 (8) | 7.38 (8) | 4.07 (8) | 0 | 0 | 8.67 (8) |
| $A_{82}$ | 8.66 (7) | 1.46 (9) | 0 | 2.82 (8) | 0 | 0 |
| $A_{83}$ | 1.44 (8) | 0 | 0 | 9.10 (7) | 0 | 0 |
| $A_{84}$ | 8.23 (4) | 0 | 0 | 7.33 (2) | 0 | 0 |
| $A_{85}$ | 5.80 (3) | 0 | 0 | 0 | 0 | 0 |
| $A_{86}$ | 0 | 0 | 0 | 0 | 3.69 (7) | 0 |
| $A_{87}$ | 0 | 0 | 0 | 0 | 1.97 (2) | 0 |
| $A_{91}$ | 0 | | 2.72 (4) | 2.10 (8) | 0 | |
| $A_{92}$ | 8.72 (7) | | 0 | 1.54 (8) | 0 | |
| $A_{93}$ | 2.61 (8) | | 3.46 (8) | 9.96 (6) | 0 | |
| $A_{94}$ | 7.70 (2) | | 8.35 (7) | 5.20 (2) | 0 | |
| $A_{95}$ | 0 | | 4.01 (7) | 3.62 (2) | 0 | |
| $A_{96}$ | 0 | | 0 | 0 | 3.69 (7) | |
| $A_{97}$ | 0 | | 0 | 0 | 3.61 (2) | |
| $A_{98}$ | 0 | | 0 | 0 | 0 | |
| $A_{10\text{-}1}$ | 3.64 (4) | | 4.94 (4) | 4.23 (8) | 0 | |
| $A_{10\text{-}2}$ | 2.80 (4) | | 3.11 (8) | 3.21 (8) | 0 | |
| $A_{10\text{-}3}$ | 2.96 (4) | | 3.26 (7) | 5.27 (8) | 0 | |

to be continued

Continued from Table 2

| Transitions | C I | C II | N I | N II | O I | O II |
|---|---|---|---|---|---|---|
| $A_{10\text{-}4}$ | 3.39 (8) | | 2.12 (7) | 5.16 (3) | 0 | |
| $A_{10\text{-}5}$ | 2.80 (7) | | 1.05 (8) | 2.06 (3) | 0 | |
| $A_{10\text{-}6}$ | 0 | | 0 | 1.15 (–2) | 3.69 (7) | |
| $A_{10\text{-}7}$ | 0 | | 0 | 3.55 (–1) | 0 | |
| $A_{10\text{-}8}$ | 0 | | 0 | 6.32 (–2) | 0 | |
| $A_{10\text{-}9}$ | 0 | | 5.17 (–6) | 3.41 (–1) | 0 | |
| $A_{11\text{-}1}$ | 0 | | 1.44 (8) | 0 | 0 | |
| $A_{11\text{-}2}$ | 0 | | 0 | 3.14 (8) | 0 | |
| $A_{11\text{-}3}$ | 1.17 (8) | | 0 | 9.55 (8) | 0 | |
| $A_{11\text{-}4}$ | 0 | | 0 | 2.30 (3) | 0 | |
| $A_{11\text{-}5}$ | 0 | | 0 | 0 | 0 | |
| $A_{11\text{-}6}$ | 0 | | 2.30 (–5) | 2.08 (–2) | 6.44 (2) | |
| $A_{11\text{-}7}$ | 0 | | 5.90 (–4) | 4.27 (–1) | 3.22 (7) | |
| $A_{11\text{-}8}$ | 0 | | 6.60 (–3) | 2.66 (–1) | 0 | |
| $A_{11\text{-}9}$ | 0 | | 0 | 6.83 (–2) | 0 | |
| $A_{11\text{-}10}$ | 0 | | 0 | 0 | 0 | |
| $A_{12\text{-}1}$ | 6.54 (7) | | 1.49 (8) | 0 | 0 | |
| $A_{12\text{-}2}$ | 4.89 (7) | | 0 | 1.27 (9) | 0 | |
| $A_{12\text{-}3}$ | 3.25 (6) | | 0 | 0 | 0 | |
| $A_{12\text{-}4}$ | 0 | | 0 | 0 | 0 | |
| $A_{12\text{-}5}$ | 0 | | 0 | 0 | 0 | |
| $A_{12\text{-}6}$ | 0 | | 4.70 (–4) | 0 | 1.18 (3) | |
| $A_{12\text{-}7}$ | 0 | | 2.80 (–3) | 0 | 3.22 (7) | |
| $A_{12\text{-}8}$ | 0 | | 4.20 (–5) | 7.60 (–1) | 0 | |
| $A_{12\text{-}9}$ | 0 | | 0 | 3.29 (–3) | 0 | |
| $A_{12\text{-}10}$ | 0 | | 0 | 0 | 0 | |
| $A_{12\text{-}11}$ | 0 | | 0 | 0 | 0 | |
| $A_{13\text{-}1}$ | 0 | | 1.51 (8) | | 0 | |
| $A_{13\text{-}2}$ | 8.82 (7) | | 1.21 (4) | | 0 | |
| $A_{13\text{-}3}$ | 2.93 (7) | | 0 | | 0 | |
| $A_{13\text{-}4}$ | 0 | | 0 | | 0 | |
| $A_{13\text{-}5}$ | 0 | | 0 | | 0 | |
| $A_{13\text{-}6}$ | 0 | | 1.20 (–3) | | 0 | |
| $A_{13\text{-}7}$ | 0 | | 7.30 (–5) | | 3.22 (7) | |
| $A_{13\text{-}8}$ | 0 | | 6.30 (–5) | | 0 | |
| $A_{13\text{-}9}$ | 0 | | 0 | | 0 | |
| $A_{13\text{-}10}$ | 0 | | 0 | | 0 | |
| $A_{13\text{-}11}$ | 0 | | 0 | | 0 | |
| $A_{13\text{-}12}$ | 0 | | 0 | | 0 | |

to be continued

Continued from Table 2

| Transitions | C I | C II | N I | N II | O I | O II |
|---|---|---|---|---|---|---|
| $A_{14\text{-}1}$ | | | 0 | | | |
| $A_{14\text{-}2}$ | | | 0 | | | |
| $A_{14\text{-}3}$ | | | 0 | | | |
| $A_{14\text{-}4}$ | | | 0 | | | |
| $A_{14\text{-}5}$ | | | 0 | | | |
| $A_{14\text{-}6}$ | | | 3.18 (3) | | | |
| $A_{14\text{-}7}$ | | | 9.03 (3) | | | |
| $A_{14\text{-}8}$ | | | 0 | | | |
| $A_{14\text{-}9}$ | | | 3.09 (6) | | | |
| $A_{14\text{-}10}$ | | | 5.73 (6) | | | |
| $A_{14\text{-}11}$ | | | 0 | | | |
| $A_{14\text{-}12}$ | | | 0 | | | |
| $A_{14\text{-}13}$ | | | 0 | | | |

where $C_{ij}$ and $C_{ji}$ are the collisional excitation coefficients (unit: $s^{-1}$) from energy state $i$ to $j$ and deexcitation coefficients ($s^{-1}$) from energy state $j$ to $i$, respectively. Based on detailed energy balance,

$$\frac{C_{ij}}{C_{ji}} = \frac{g_j}{g_i}\mathrm{e}^{-\frac{E_j-E_i}{kT}}\ (j>i),$$

$N_j\sum_{i=1}^{j-1}A_{ji}$ are the spontaneous emission rates from energy state $j$ to $i$. $N_j\sum_{i=1}^{j-1}C_{ji}$ is the sum of all collisional deexcitation rates from $j$ to energy states $i<j$, and $N_j\sum C_{jk}$ are the collisional excitation rates from $j$ to energy states $k>j$.

Photoexcitation, photo-deexcitation and chemical reactions processes are ignored in this work. Photoexcitation should increase the population of high energy states, which would enhance emission from the considered metal species and strengthen our main conclusion that metal cooling could be important in the upper atmosphere of close-in exoplanets. Photo-deexcitation will also strengthen this conclusion because the decrease of excited state populations through this process is accomplished by emissions, again contributing to cooling. Since their consideration could only strengthen our already significant findings, it is reasonable to neglect these processes in this work. A further simplification is that collisional excitations from excited energy states are ignored. When the ground energy state contains several fine structure energy levels, the excitations from all fine structure levels are included.

Assuming that the velocities of the impactors ($V$) follow the Maxwellian distribution $f(V)=4\pi\left(\frac{m}{2\pi kT}\right)^{1.5}V^2\mathrm{e}^{\frac{-mV^2}{2kT}}$, where $m$ is the mass of the impactor, and that excitations from energy level $i$ to $j$ occur only when $V\geq V_0=\sqrt{\frac{2hE_{ij}}{m}}$, the collisional excitation coefficient $C_{ij}$ is

$$C_{ij}=nV\int_{v_0}^{\infty}\sigma(V)f(V)\,\mathrm{d}V=4\pi n\left(\frac{m}{2\pi kT}\right)^{1.5}\int_{V_0}^{\infty}\sigma(V)V^3\mathrm{e}^{\frac{-mV^2}{2kT}}\,\mathrm{d}V, \quad (2)$$

where $n$ is the number density of the impactors and $\sigma$ are the collisional excitation cross sections.

In this work, we adopt electron-impact excitation cross sections from the literature (see the Supplementary Materials for details). To evaluate the effect of metal emissions due to collisions with background neutral particles or ions, we assume that the excitation and deexcitation cross sections of such neutral-impact collisions are 4 times those of their corresponding electron-impact collisions because the collision radius of neutral impact collision should be twice that of electron impact collision if all collisional particles are considered as hard spheres. We further assume that neutral-impact collisions deliver half the kinetic energy of the impactors to the targets, which maximizes the significance of emissions induced by neutral-impact collisions and the subsequent radiative cooling effect (see the Supplementary Materials for the derivations).

### 2.2 Monte Carlo Model

The population balance model is based on analytical solution of the equilibrium equations between collisional excitation, collisional deexcitation, and spontaneous emissions. While the solutions are robust, it is difficult to add new energy levels to the model. Thus, we developed a Monte Carlo model to explicitly simulate the equilibrium results of collisional processes of multiple particles.

The basic consideration for energy states is the same in the Monte Carlo model as that in the population balance model. The Monte Carlo model assumes that all particles are initially at the ground energy state. Then, based on collisional frequency, the model predicts the time required for each particle to have a collision. Once a

collisional excitation occurs, the model uses the specific collisional excitation cross sections to predict to which energy states the particle should be excited. For particles at the excited states, the model also calculates the time for the particle to be collisionally deexcited, the destination energy states, and the time for the particle to experience a spontaneous emission. All test particles are simulated in this fashion until the population distribution of all particles does not change with time. A typical simulation model time is $10^7$ seconds which depends on density and temperature. The emission rates and the final population distribution obtained from the Monte Carlo model are consistent with those from the population balance model.

### 2.3 Model Validation

We further validate our models against the classical fine structure emission of O I in modern Earth's upper atmosphere (Kockarts and Peetermans, 1970) (KP70 in the following), which assumes Boltzmann distribution for the lowest 3 energy states of O I. The typical profiles of electron temperature ($T_e$), neutral temperature ($T_n$), electron density ($n_e$), and O I density (the most abundant atomic species) in modern Earth's thermosphere under solar maximum conditions (Tian F et al., 2008b) are used as inputs in our model.

The black curve in Figure 1 is the O I emission calculated using the classical KP70 formula, which is widely used in Earth upper atmosphere models (Roble et al., 1987; Roble, 1995; Tian F et al., 2008a). The blue curve in Figure 1 is the O I fine structure emission assuming Boltzmann distribution with all 13 energy states (used in our models). We can see that the KP70 formula is a good approximation for the cooling in the lower thermosphere of modern Earth. We note that the total O I emission in modern Earth's upper thermosphere is slightly stronger than O I 63 micron because of the contributions in other emission lines (not shown in Figure 1).

The orange curve in Figure 1 is the O I fine structure emission calculated by the population balance model when considering electron-impact effects only. The red curve is the O I fine structure emission in the population balance model when considering both electron-O I collisions and O I-O I collisions. We can draw two conclusions from Figure 1: 1) The two curves do not overlap completely: O I-O I collisions in modern Earth's thermosphere are non-negligible when considering O I fine structure emission; 2) The red curve deviates from the blue and the black ones at altitude > 400 km: O I emission calculated in the population balance model is weaker than that from assuming a Boltzmann distribution because collisions in modern Earth's upper thermosphere are not frequent enough to ensure a Boltzman distribution of O I. Thus, one cannot safely assume Boltzmann distribution when considering metal emissions from planetary upper atmospheres of close-in exoplanets. We conclude that our models are valid for modern Earth's thermosphere and proper physics has been included in our models. Thus although the environments of close-in exoplanets and the Earth are different, in the following we apply our models to the extreme conditions found in these planets as a first order approximation.

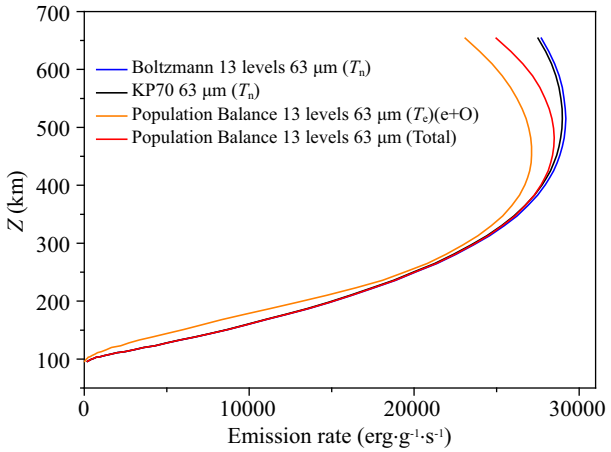


**Figure 1**. Comparison of O I emission in modern Earth's thermosphere between Boltzmann assumption and our population balance model in solar maximum condition. The black curve represents O I 63 μm emission using KP70 formula (Kockarts and Peetermans, 1970) and $T_n$. The blue curve represents O I 63 μm emission assuming 13 energy states following the Boltzmann distribution under $T_n$. The orange curve represents O I 63 μm emission in the population balance model considering only electron collisions. The red curve represents results of a population balance model calculation including both neutral collisions and electrons collisions.

## 3. Results and Conclusions

Our first result is that metal emissions due to electron collisions are strong non-linear functions of $T_e$ (Figure 2 for $n_e$=$10^6$ cm$^{-3}$ cases; for $n_e$=$10^3$ cm$^{-3}$ cases, see Supplementary Materials). When increasing $T_e$ from 3×$10^3$ to $10^4$ K, emissions of O I, C I, and N I in-

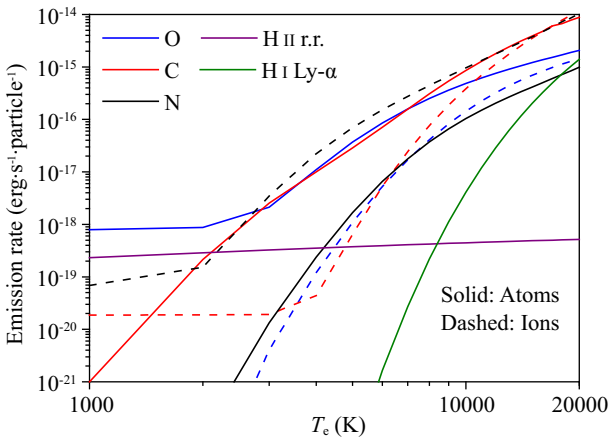


**Figure 2**. Emissions of H II radiative recombination (r. r.), H I Ly-α, and metals (C, N, O) induced by electron collisions at $n_e$=$10^6$ cm$^{-3}$. Emissions of atoms and ions are shown as solid and dashed curves respectively. The most important metal emissions are 63 and 0.63 μm lines for O I, 0.73, 0.37, and 0.25 μm for O II, 370, 0.98, 0.87, and 0.3 μm for C I, 158 and 0.23 μm for C II, 1.0, 0.52, 0.11/0.12 μm for N I, and 205, 0.66, 0.58, and 0.21 μm for N II (122 μm could become important in some $n_e$ cases, see Supplementary Materials). If metals are with similar abundances as those of H II and H I, metal cooling would dominate that of H.

crease by 2, 3, and 4 orders of magnitude, respectively (Figure 2). It is interesting that while N I has much weaker emission capability than N II, C I and O I are much stronger emitters than their corresponding ions at $T_e<10^4$ K. Thus, ionosphere chemistry can play an important role in the energy budgets of planetary upper atmospheres under intense stellar XUV radiation.

The emissions from H II radiative recombination (Murray-Clay et al., 2009; Seaton, 1959) and H I Ly-$\alpha$ (Glover and Jappsen, 2007; Black, 1981) are also shown in Figure 2. It is clear that the emission capabilities of metals are stronger than that of hydrogen species if their abundances are comparable. While H is the most abundant species in the atmosphere of Jupiter-mass and Neptune-mass planets, and its mixing ratio is not well constrained in rocky planets; therefore the significance of metal cooling cannot be appropriately determined in Figure 2. To demonstrate this, the ratios between the number densities of metals and H at which metal emissions (functions of $T_e$ and $n_e$) are equal to the sum of H II recombination and H I Ly-$\alpha$ (also functions of $T_e$ and $n_e$) are shown in Figure 3. For simplicity, we assume $n_H \sim n_{H^+}$ for Figure 3. The yellow and red regions mark the regions where metal abundances are 10~100 times lower than that of H. The relevant observations of planetary upper atmosphere environments are: the peak temperature in hot Jupiters' upper atmospheres are $>10^4$ K (Murray-Clay et al., 2009; Koskinen et al., 2013a; Yelle, 2004; Owen and Jackson, 2012) and the O I/H II ratios near the $T$ peak region in the upper atmospheres of hot Jupiters are $>10^{-2}$ (Koskinen et al., 2013a). Thus Figure 3 clearly shows that metal emissions could be important in a large parameter space.

More quantitatively, the radiative cooling rate near the $T$ peak is on the order of $10^{-9}$ erg·cm$^{-3}$·s$^{-1}$ (Koskinen et al., 2013a). The emission rate of O I at $T_e>10^4$ K is close to $10^{-15}$ erg·s$^{-1}$·particle$^{-1}$ (Figure 2). Because O I density is $10^5$~$10^6$ cm$^{-3}$ near the $T$ peak in the upper atmosphere of hot Jupiters (Koskinen et al., 2013a), O I emission should be at least 10% of H cooling. We note that the peak temperature in the above analysis refers to neutral temperature $T_n$; because typically $T_e>T_n$, metal emissions could be even more significant in comparison to H emission than Figure 3 demonstrates.

One important feature of metal emissions is that some of the most important emissions are in the visible and near-IR range. At $n_e=10^6$ cm$^{-3}$, these emissions (shown in Figure 4) include O I's 0.63 μm ($T_e>3\times10^3$ K), O II's 0.73 μm ($T_e>7\times10^3$ K), N I's 1.00 μm ($T_e>4\times10^3$ K), N II's 0.66 μm ($T_e>2\times10^3$ K), C I's 0.98 μm ($T_e>1\times10^3$ K), and O I's 0.87 μm ($T_e>7\times10^3$ K). In comparison, H II radiative recombination emits in the EUV wavelength range and H I Ly-$\alpha$ emission is in the FUV range, both of which could be absorbed by planetary upper atmospheres. Thus, metal emissions should be taken into account in the energy budget of planetary upper atmospheres under strong XUV radiation.

In order to facilitate the implementation of metal emissions in planetary upper atmosphere models, relationships between log ($n_e$) and log ($F$) are found with $T_e$-dependent 5-term polynomial functions; the fitting parameters are given in Table 3.

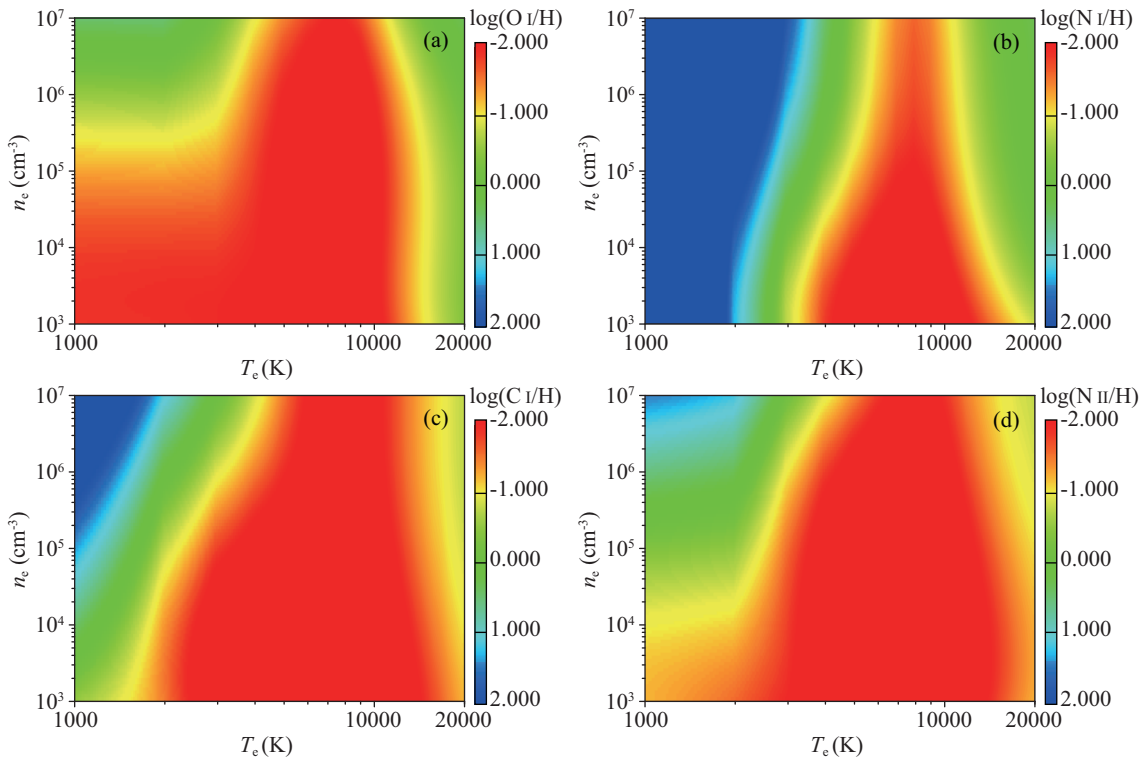


**Figure 3**. Conditions for metal emissions to be identical to the sum of H II recombination cooling plus H I Ly-α cooling. For simplicity purpose $n_H \sim n_{H^+}$ is assumed. log(metal/H)=-2 means that density of metal is 1% that of H. C/N/O are more efficient radiators than H in large parameter spaces, indicating strong cooling potential from metals in the upper atmospheres of close-in planets.

Assuming $T_e$=$T_n$, Figure 5 shows the ratio of total metal emission $E_{total}$ (including both electron-collision-induced and neutral-collision-induced) and electron-induced metal emissions ($E_e$) for O I at $10^3$ and $10^4$ K, C I at $10^4$ K, and N II at $10^4$ K respectively. For O I at $10^3$ K, the effect of neutral collisions is small if $n_e$ is greater than $10^5$ cm$^{-3}$. For O I at $10^4$ K, neutral collisions become important for O I emissions when $n_e$ is close to $10^6$ cm$^{-3}$. For C I and N II, neutral collisions could also become important in density ranges possible for planetary upper atmospheres under strong XUV radiation (Tian F et al., 2008a, b, 2009; Koskinen et al., 2013a). Note that the assumption that $T_n$=$T_e$ is not satisfied in most planetary upper atmospheres; Figure 5 thus serves only as an indication of the potential significance of neutral-induced metal emissions.

We calculate $E_{total}/E_e$ for a wide range of $T_n$ and $T_e$ and the results are fitted to 6-term polynomial functions with fitting parameters included in Table 4. Combining Tables 3 and 4, total metal emissions can be calculated. We caution that these are optimistic estimates because of our simplifications for neutral-induced emissions.

Close-in mini-Neptunes could lose their H/He envelopes through photoevaporation and evolve into gas-poor super Earths (Lopez et al., 2012; Tian F, 2015). Metal emissions should be important on such planets because atmospheric metal abundances should increase dramatically during this evolution. Efficient metal emissions could also have interesting implications for the fate of water inventories on rocky planets orbiting M dwarfs. It is suggested that rapid water loss could result in the buildup of massive $O_2$ atmospheres on such planets as a result of early luminosity evolution of M dwarfs (Luger et al., 2015; Tian F, 2015). A recent model studying the early evolution of GJ 1132b shows that $O_2$ is more abundant than water vapor in the atmosphere even when considering efficient reactions of atmospheric $O_2$ with magma ocean (Schaefer et al., 2016). In such a scenario, efficient metal emission could result in negative feedback on water loss, which could help to preserve planet water inventory.

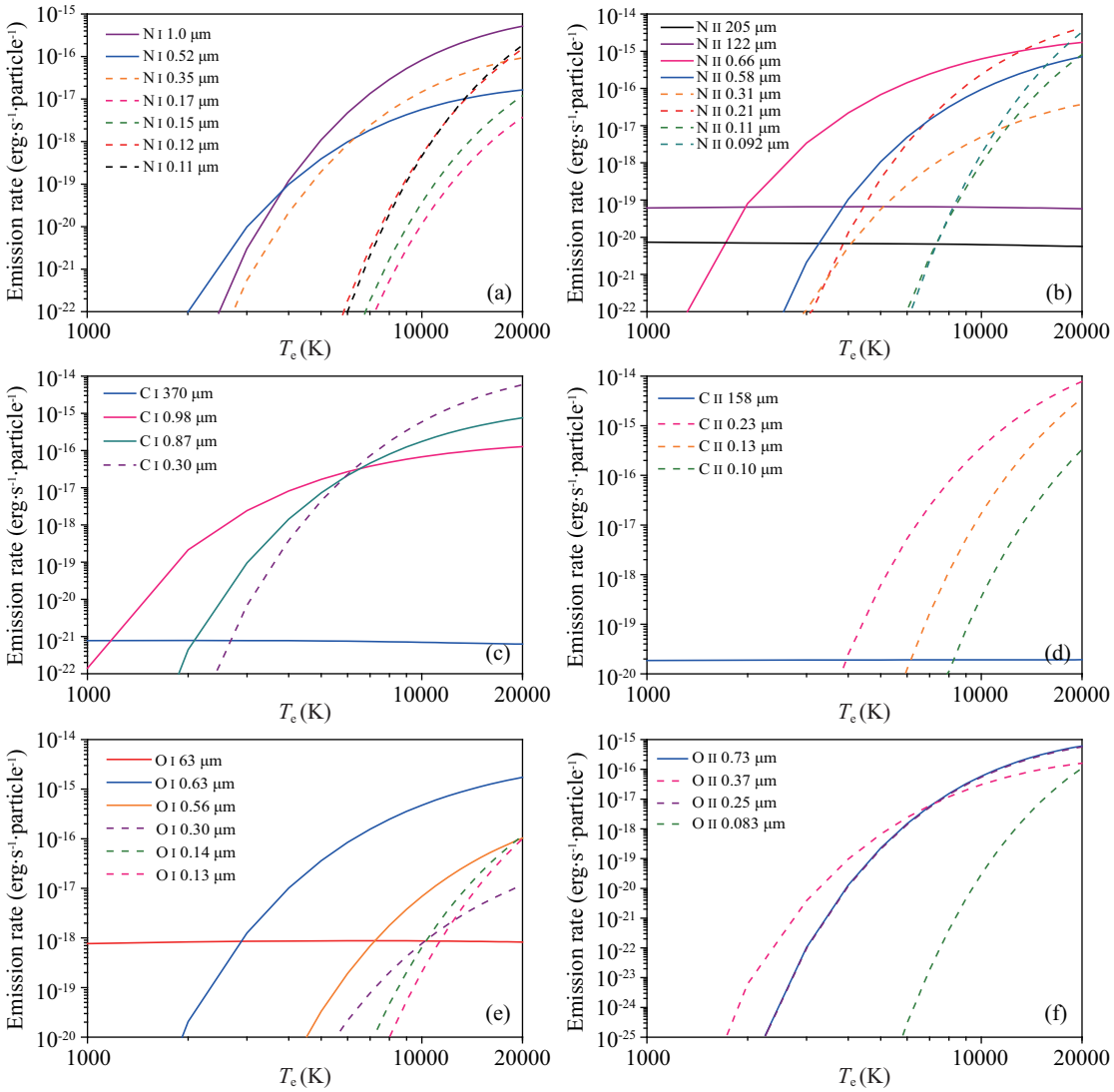


**Figure 4**. Metal emission rates for $n_e$=$10^6$ cm$^{-3}$. For each metal species only the most important emission lines are shown. The dashed lines represent that the emissions are UV emissions.

**Table 3.** Polynomial fit for metal emissions considering electron collisions for $10^3$ cm$^{-3}$ < $n_e$ < $10^8$ cm$^{-3}$

$$\log(E_e) = R_0 + R_1 \times \log(n_e) + R_2 \times \log^2(n_e) + R_3 \times \log^3(n_e) + R_4 \times \log^4(n_e)$$

note: the unit of $E_e$ is erg·particle$^{-1}$·s$^{-1}$

| $T$ (K) | Parameters | C I | N I | O I | C II | N II | O II |
|---|---|---|---|---|---|---|---|
| 1000 | $R_0$ | –2.10 (1) | –3.78 (1) | –2.53 (1) | –1.98 (1) | –2.72 (1) | –2.63 (1) |
| | $R_1$ | –1.23 (1) | 5.81 | 2.54 | 3.02 (–2) | 3.92 | 3.46 |
| | $R_2$ | 5.51 (–2) | –1.29 | –2.18 (–1) | –7.31 (–3) | –6.96 (–1) | –5.41 (–1) |
| | $R_3$ | –7.63 (–3) | 1.25 (–1) | –8.10 (–3) | 7.69 (–4) | 5.28 (–2) | 3.31 (–2) |
| | $R_4$ | 3.44 (–4) | –4.52 (–3) | 1.22 (–3) | –2.97 (–5) | –1.42 (–3) | –5.64 (–4) |
| 5000 | $R_0$ | –3.37 (1) | –2.54 (1) | –1.68 (1) | –1.52 (1) | –1.81 (1) | –3.25 (1) |
| | $R_1$ | 1.13 (1) | 5.59 | –3.13 | –3.08 | –2.39 | 9.62 |
| | $R_2$ | –2.88 | –1.75 | 1.15 | 6.29 (–1) | 1.22 | –2.50 |
| | $R_3$ | 3.20 (–1) | 2.43 (–1) | –1.34 (–1) | –3.59 (–2) | –1.82 (–1) | 2.90 (–1) |
| | $R_4$ | –1.27 (–2) | –1.17 (–2) | 5.10 (–3) | 4.17 (–4) | 8.75 (–3) | –1.23 (–2) |
| 10000 | $R_0$ | –2.60 (1) | –1.48 (1) | –1.33 (1) | –2.16 (1) | –2.58 (1) | –2.82 (1) |
| | $R_1$ | 6.36 | –1.93 | –5.53 | 1.18 | 4.90 | 7.83 |
| | $R_2$ | –1.67 | 3.71 (–1) | 1.95 | –7.05 (–2) | –8.94 (–1) | –2.12 |
| | $R_3$ | 2.06 (–1) | –4.22 (–3) | –2.43 (–1) | 1.07 (–2) | 7.53 (–2) | 2.66 (–1) |
| | $R_4$ | –8.95 (–3) | –1.42 (–3) | 1.04 (–2) | –5.67 (–4) | –2.03 (–3) | –1.20 (–2) |
| 15000 | $R_0$ | –2.21 (1) | –1.07 (1) | –1.41 (1) | –2.08 (1) | –2.60 (1) | –2.57 (1) |
| | $R_1$ | 3.44 | –5.17 | –4.73 | 1.32 | 5.68 | 6.28 |
| | $R_2$ | –8.42 (–1) | 1.39 | 1.78 | –1.01 (–1) | –1.22 | –1.70 |
| | $R_3$ | 1.10 (–1) | –1.37 (–1) | –2.33 (–1) | 1.35 (–2) | 1.27 (–1) | 2.19 (–1) |
| | $R_4$ | –5.01 (–3) | 4.83 (–3) | 1.05 (–2) | –6.53 (–4) | –4.67 (–3) | –1.01 (–2) |
| 20000 | $R_0$ | –2.07 (1) | –1.14 (1) | –1.69 (1) | –2.03 (1) | –2.43 (1) | –2.33 (–1) |
| | $R_1$ | 2.40 | –4.72 | –2.22 | 1.29 | 4.66 | 4.55 |
| | $R_2$ | –5.26 (–1) | 1.33 | 1.07 | –8.85 (–2) | –9.82 (–1) | –1.20 |
| | $R_3$ | 7.20 (–2) | –1.37 (–1) | –1.48 (–1) | 1.17 (–2) | 1.07 (–1) | 1.56 (–1) |
| | $R_4$ | –3.36 (–3) | 5.12 (–3) | 7.02 (–3) | –5.67 (–4) | –4.13 (–3) | –7.19 (–3) |

In this work, we consider only C, N, O, and their ions. Although absorptions of Na and K in exoplanetary atmospheres have been observed (Sing et al., 2011, 2008a, b ; Charbonneau et al., 2002), their emissions have not yet been detected. The locations of observed Na/K absorption are at $10^{-6}$ bar pressure level (Sing et al., 2011, 2008b), which is much lower than the typical lower boundary of planetary upper atmospheres. Although the radiation capability of a single Na atom far exceeds that of C/N/O, the overall cooling capability of Na should be small. The excitation cross section of Na from the ground state to its first excitation state ($^2P^o$, 2.1 eV) is on the order of $10^{-15}$ cm$^2$ (Shuker et al., 1980). Assuming a $T_e$ of $10^4$ K, an $n_e$ of $10^6$ cm$^{-3}$, and that every excitation leads to a photon emission of 2.1 eV energy, the emission of Na is on the order of $10^{-14}$ erg·s$^{-1}$·particle$^{-1}$. The emission of C/N/O and their ions are on the order of $10^{-15}$ erg·s$^{-1}$·particle$^{-1}$ in the same environment (Figure 2). Given that typically Na is much less abundant than C/N/O, it appears that the emission of Na in planetary upper atmospheres as a cooling mechanism can be ignored. Thus, it is a good approximation to consider metal cooling from C, N, and O first.

The influence of ionization fraction can be calculated when considering a complete ionosphere model including relevant ionization and recombination processes. Such a model is necessary to evaluate the importance of atmospheric escape on planet evolution as well, which will be an important future work. In this work, the cooling capabilities of neutral C, N, O atoms and their single-ionized ions are calculated without assuming the Boltzmann distribution. Fitting formula and parameters are provided so that the total cooling from these metal species could be included in future ionosphere and thermosphere models. Future exoplanet observations could provide interesting observation constraints.

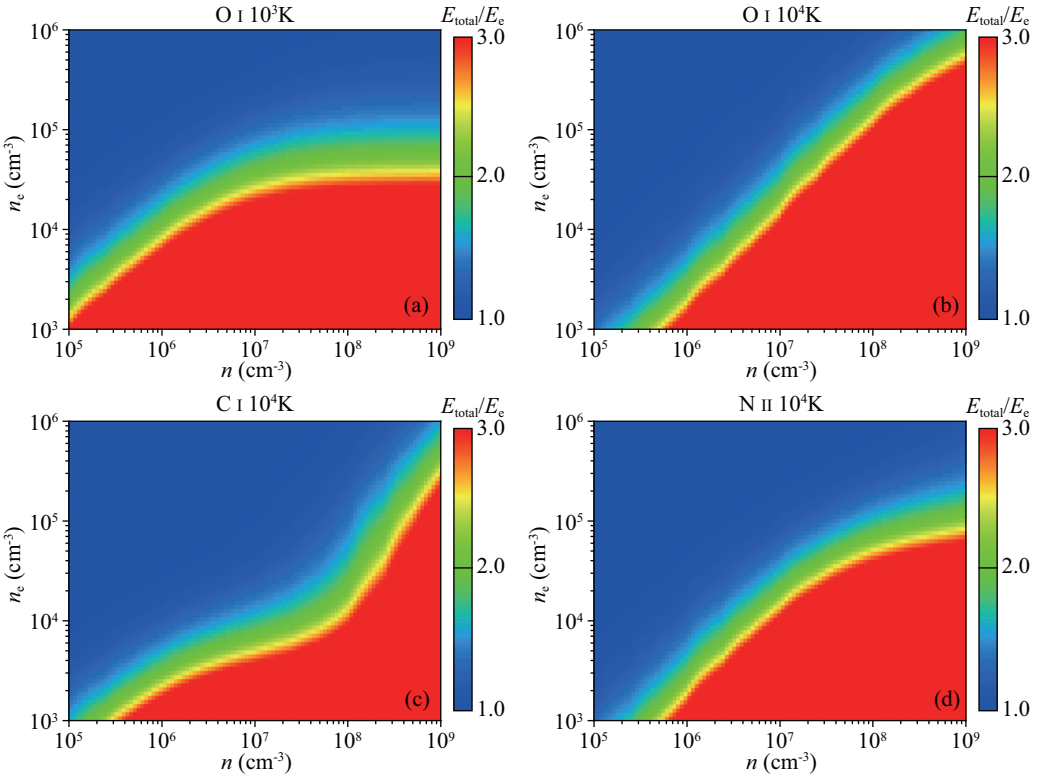


**Figure 5**. $E_{total}/E_e$ at different $T_e$ for O I at $10^3$ (panel a) and $10^4$ K (panel b), C I at $10^4$ K (panel c) and N II at $10^4$ K (panel d), respectively.

**Table 4.** Polynomial fit for $E_{total}/E_e$ for $10^5$ cm$^{-3}$ < $n$ < $10^9$ cm$^{-3}$, where $E_{total}$ represents metal emissions considering all collisions

$$E_{total}/E_e = R_0 + R_1 \times \log(n) + R_2 \times \log^2(n) + R_3 \times \log^3(n) + R_4 \times \log^4(n) + R_5 \times \log^5(n)$$

| Particles | $T_n$ (K) | $T_e$ (K) | Parameters | $n_e$ (cm$^{-3}$) | | | | | | |
|---|---|---|---|---|---|---|---|---|---|---|
| | | | | $10^3$ | $5\times10^3$ | $10^4$ | $5\times10^4$ | $10^5$ | $5\times10^5$ | $10^6$ |
| C I | 3000 | 3000 | $R_0$ | 1.23 (3) | 3.37 (2) | 2.02 (2) | 3.84 (1) | 1.14 (1) | 4.87 (–1) | 7.44 (–1) |
| | | | $R_1$ | –1.02 (3) | –2.71 (2) | –1.59 (2) | –2.86 (1) | –7.83 | 4.17 (–1) | 2.03 (–1) |
| | | | $R_2$ | 3.37 (2) | 8.67 (1) | 5.00 (1) | 8.66 | 2.32 | –1.35 (–1) | –6.42 (–2) |
| | | | $R_3$ | –5.48 (1) | –1.37 (1) | –7.76 | –1.29 | –3.37 (–1) | 2.19 (–2) | 1.01 (–2) |
| | | | $R_4$ | 4.38 | 1.07 | 5.95 (–1) | 9.53 (–2) | 2.40 (–2) | –1.17 (–3) | –7.92 (–4) |
| | | | $R_5$ | –1.38 (–1) | –3.28 (–2) | –1.80 (–2) | –2.76 (–3) | –6.67 (–4) | 5.69 (–5) | 2.47 (–5) |
| | | 5000 | $R_0$ | 7.49 (1) | –4.83 (1) | –7.91 (1) | –6.79 (1) | –2.76 (1) | 1.12 (1) | 7.55 |
| | | | $R_1$ | –6.14 (1) | 3.94 (1) | 6.30 (1) | 5.23 (1) | 2.11 (1) | –8.15 | –5.18 |
| | | | $R_2$ | 2.01 (1) | –1.25 (1) | –1.96 (1) | –1.57 (1) | –6.10 | 2.60 | 1.63 |
| | | | $R_3$ | –3.26 | 1.96 | 3.02 | 2.32 | 8.62 (–1) | –4.14 (–1) | –2.55 (–1) |
| | | | $R_4$ | 2.60 (–1) | –1.52 (–1) | –2.30 (–1) | –1.69 (–1) | –5.92 (–2) | 3.28 (–2) | 1.99 (–2) |
| | | | $R_5$ | –8.15 (–3) | 4.63 (–3) | 6.90 (–3) | 4.83 (–3) | 1.56 (–3) | –1.04 (–3) | –6.19 (–4) |
| | | 10000 | $R_0$ | –4.07 (1) | –8.34 (1) | –9.24 (1) | –3.29 (1) | –5.06 | 1.50 | 5.52 (–1) |
| | | | $R_1$ | 3.45 (1) | 6.70 (1) | 7.30 (1) | 2.55 (1) | 4.25 | –3.96 (–1) | 3.53 (–1) |
| | | | $R_2$ | –1.13 (1) | –2.11 (1) | –2.26 (1) | –7.58 | –1.15 | 1.25 (–1) | –1.11 (–1) |
| | | | $R_3$ | 1.81 | 3.28 | 3.45 | 1.11 | 1.48 (–1) | –1.98 (–2) | 1.73 (–2) |
| | | | $R_4$ | –1.44 (–1) | –2.52 (–1) | –2.61 (–1) | –7.93 (–2) | –8.80 (–3) | 1.55 (–3) | –1.35 (–3) |
| | | | $R_5$ | 4.50 (–3) | 7.63 (–3) | 7.77 (–3) | 2.22 (–3) | 1.79 (–4) | –4.86 (–5) | 4.17 (–5) |

to be continued

Continued from Table 4

$E_{total}/E_e = R_0 + R_1 \times \log(n) + R_2 \times \log^2(n) + R_3 \times \log^3(n) + R_4 \times \log^4(n) + R_5 \times \log^5(n)$

| Particles | $T_n$ (K) | $T_e$ (K) | Parameters | $n_e$ (cm$^{-3}$) | | | | | | |
|---|---|---|---|---|---|---|---|---|---|---|
| | | | | $10^3$ | $5\times10^3$ | $10^4$ | $5\times10^4$ | $10^5$ | $5\times10^5$ | $10^6$ |
| C I | 10000 | 10000 | $R_0$ | –7.19 (3) | –2.09 (3) | –1.42 (3) | –6.59 (2) | –4.45 (2) | –1.32 (2) | –6.98 (1) |
| | | | $R_1$ | 5.77 (3) | 1.66 (3) | 1.12 (3) | 5.18 (2) | 3.50 (2) | 1.04 (2) | 5.55 (1) |
| | | | $R_2$ | –1.84 (3) | –5.26 (2) | –3.52 (2) | –1.62 (2) | –1.09 (2) | –3.26 (1) | –1.73 (1) |
| | | | $R_3$ | 2.91 (2) | 8.26 (1) | 5.51 (1) | 2.51 (1) | 1.69 (1) | 5.06 | 2.69 |
| | | | $R_4$ | –2.29 (1) | –6.45 | –4.28 | –1.93 | –1.31 | –3.91 (–1) | –2.08 (–1) |
| | | | $R_5$ | 7.15 (–1) | 2.00 (–1) | 1.32 (–1) | 5.94 (–2) | 4.02 (–2) | 1.20 (–2) | 6.40 (–3) |
| | | 15000 | $R_0$ | –3.45 (3) | –9.91 (2) | –6.33 (2) | –2.08 (2) | –1.25 (2) | –2.73 (1) | –6.30 |
| | | | $R_1$ | 2.76 (3) | 7.85 (2) | 4.99 (2) | 1.64 (2) | 9.90 (1) | 2.20 (1) | 5.71 |
| | | | $R_2$ | –8.78 (2) | –2.47 (2) | –1.56 (2) | –5.12 (1) | –3.09 (1) | –6.78 | –1.78 |
| | | | $R_3$ | 1.39 (2) | 3.86 (1) | 2.43 (1) | 7.97 | 4.81 | 1.04 | 2.78 (–1) |
| | | | $R_4$ | –1.09 (1) | –3.00 | –1.88 | –6.17 (–1) | –3.72 (–1) | –7.96 (–2) | –2.18 (–2) |
| | | | $R_5$ | 3.40 (–1) | 9.28 (–2) | 5.78 (–2) | 1.91 (–2) | 1.15 (–2) | 2.43 (–3) | 6.87 (–4) |
| | | 20000 | $R_0$ | –2.17 (3) | –6.08 (2) | –3.69 (2) | –1.09 (2) | –7.13 (1) | –7.07 | 9.80 |
| | | | $R_1$ | 1.73 (3) | 4.80 (2) | 2.90 (2) | 8.63 (1) | 5.64 (1) | 5.83 | –6.93 |
| | | | $R_2$ | –5.51 (2) | –1.51 (2) | –9.06 (1) | –2.69 (1) | –1.75 (1) | –1.66 | 2.15 |
| | | | $R_3$ | 8.69 (1) | 2.35 (1) | 1.41 (1) | 4.19 | 2.68 | 2.35 (–1) | –3.30 (–1) |
| | | | $R_4$ | –6.81 | –1.82 | –1.09 | –3.23 (–1) | –2.05 (–1) | –1.66 (–2) | 2.48 (–2) |
| | | | $R_5$ | 2.12 (–1) | 5.62 (–2) | 3.34 (–2) | 9.96 (–3) | 6.25 (–3) | 4.75 (–4) | –7.28 (–4) |
| N I | 10000 | 10000 | $R_0$ | –3.06 (3) | –1.48 (3) | –1.17 (3) | –6.21 (2) | –4.16 (2) | –1.14 (2) | –5.88 (1) |
| | | | $R_1$ | 2.43 (3) | 1.16 (3) | 9.22 (2) | 4.88 (2) | 3.27 (2) | 9.03 (1) | 4.69 (1) |
| | | | $R_2$ | –7.64 (2) | –3.63 (2) | –2.88 (2) | –1.52 (2) | –1.02 (2) | –2.82 (1) | –1.46 (1) |
| | | | $R_3$ | 1.20 (2) | 5.64 (1) | 4.46 (1) | 2.36 (1) | 1.58 (1) | 4.37 | 2.27 |
| | | | $R_4$ | –9.30 | –4.36 | –3.44 | –1.82 | –1.22 | –3.37 (–1) | –1.75 (–1) |
| | | | $R_5$ | 2.88 (–1) | 1.34 (–1) | 1.06 (–1) | 5.60 (–2) | 3.75 (–2) | 1.04 (–2) | 5.38 (–3) |
| | | 15000 | $R_0$ | –1.23 (3) | –5.46 (2) | –3.85 (2) | –1.93 (2) | –1.19 (2) | –8.80 | –4.19 |
| | | | $R_1$ | 9.69 (2) | 4.28 (2) | 3.04 (2) | 1.53 (2) | 9.37 (1) | 8.07 | 4.45 |
| | | | $R_2$ | –3.03 (2) | –1.33 (2) | –9.51 (1) | –4.79 (1) | –2.91 (1) | –2.66 | –1.52 |
| | | | $R_3$ | 4.70 (1) | 2.06 (1) | 1.48 (1) | 7.45 | 4.51 | 4.39 (–1) | 2.59 (–1) |
| | | | $R_4$ | –3.63 | –1.59 | –1.15 | –5.77 (–1) | –3.47 (–1) | –3.63 (–2) | –2.20 (–2) |
| | | | $R_5$ | 1.12 (–1) | 4.90 (–2) | 3.57 (–2) | 1.78 (–2) | 1.07 (–2) | 1.20 (–3) | 7.46 (–4) |
| | | 20000 | $R_0$ | –7.83 (2) | –3.06 (2) | –2.13 (2) | –1.09 (2) | –3.47 (1) | 2.59 (1) | 7.61 |
| | | | $R_1$ | 6.12 (2) | 2.40 (2) | 1.69 (2) | 8.49 (1) | 2.69 (1) | –1.86 (1) | –4.48 |
| | | | $R_2$ | –1.90 (2) | –7.49 (1) | –5.31 (1) | –2.60 (1) | –8.06 | 5.46 | 1.15 |
| | | | $R_3$ | 2.94 (1) | 1.16 (1) | 8.32 | 3.96 | 1.20 | –7.86 (–1) | –1.35 (–1) |
| | | | $R_4$ | –2.26 | –9.01 (–1) | –6.49 (–1) | –3.00 (–1) | –8.99 (–2) | 5.52 (–2) | 6.65 (–3) |
| | | | $R_5$ | 6.92 (–2) | 2.79 (–2) | 2.02 (–2) | 9.05 (–3) | 2.70 (–3) | –1.50 (–3) | –7.35 (–5) |

to be continued

Continued from Table 4

$E_{total}/E_e = R_0 + R_1 \times \log(n) + R_2 \times \log^2(n) + R_3 \times \log^3(n) + R_4 \times \log^4(n) + R_5 \times \log^5(n)$

| Particles | $T_n$ (K) | $T_e$ (K) | Parameters | $n_e$ (cm$^{-3}$) | | | | | | |
|---|---|---|---|---|---|---|---|---|---|---|
| | | | | $10^3$ | $5\times10^3$ | $10^4$ | $5\times10^4$ | $10^5$ | $5\times10^5$ | $10^6$ |
| O I | 1000 | 1000 | $R_0$ | –2.19 (2) | –2.36 (2) | –2.10 (2) | –1.74 (2) | –1.20 (2) | –1.74 (1) | –5.11 (–1) |
| | | | $R_1$ | 5.75 (2) | 2.67 (2) | 2.05 (2) | 1.40 (2) | 9.41 (1) | 1.34 (1) | 7.56 (–1) |
| | | | $R_2$ | –2.94 (2) | –1.06 (2) | –7.50 (1) | –4.42 (1) | –2.88 (1) | –3.84 | –9.17 (–2) |
| | | | $R_3$ | 6.06 (1) | 1.93 (1) | 1.30 (1) | 6.82 | 4.32 | 5.36 (–1) | –9.10 (–3) |
| | | | $R_4$ | –5.55 | –1.65 | –1.07 | –5.15 (–1) | –3.19 (–1) | –3.64 (–2) | 2.50 (–3) |
| | | | $R_5$ | 1.88 (–1) | 5.35 (–2) | 3.37 (–2) | 1.52 (–2) | 9.21 (–3) | 9.64 (–4) | –1.28 (–4) |
| | | 3000 | $R_0$ | –2.06 (2) | –1.84 (2) | –1.77 (2) | –1.08 (2) | –5.92 (1) | 7.86 (–1) | 4.98 (–1) |
| | | | $R_1$ | 4.01 (2) | 1.92 (2) | 1.61 (2) | 8.58 (1) | 4.60 (1) | 1.56 (–1) | 4.78 (–1) |
| | | | $R_2$ | –1.93 (2) | –7.29 (1) | –5.60 (1) | –2.65 (1) | –1.39 (1) | –4.46 (–2) | –1.75 (–1) |
| | | | $R_3$ | 3.88 (1) | 1.29 (1) | 9.33 | 4.02 | 2.05 | 6.24 (–3) | 3.11 (–2) |
| | | | $R_4$ | –3.50 | –1.08 | –7.48 (–1) | –2.99 (–1) | –1.49 (–1) | –4.27 (–4) | –2.67 (–3) |
| | | | $R_5$ | 1.18 (–1) | 3.45 (–2) | 2.32 (–2) | 8.73 (–3) | 4.26 (–3) | 1.14 (–5) | 8.91 (–5) |
| | | 5000 | $R_0$ | –8.53 (1) | –6.91 (1) | –5.87 (1) | –1.92 (1) | –6.24 | 1.07 | 9.11 (–1) |
| | | | $R_1$ | 1.54 (2) | 6.98 (1) | 5.27 (1) | 1.58 (1) | 5.50 | –4.32 (–2) | 7.59 (–2) |
| | | | $R_2$ | –7.23 (1) | –2.58 (1) | –1.79 (1) | –4.84 | –1.65 | 1.08 (–2) | –2.55 (–2) |
| | | | $R_3$ | 1.44 (1) | 4.50 | 2.95 | 7.29 (–1) | 2.43 (–1) | –1.23 (–3) | 4.20 (–3) |
| | | | $R_4$ | –1.29 | –3.72 (–1) | –2.34 (–1) | –5.39 (–2) | –1.75 (–2) | 6.17 (–5) | –3.41 (–4) |
| | | | $R_5$ | 4.33 (–2) | 1.18 (–2) | 7.20 (–3) | 1.56 (–3) | 4.98 (–4) | –9.35 (–7) | 1.08 (–5) |
| | 3000 | 3000 | $R_0$ | 2.52 (3) | 4.58 (2) | 1.78 (2) | –5.55 (1) | –5.96 (1) | –1.05 (1) | –1.34 |
| | | | $R_1$ | –1.63 (3) | –2.83 (2) | –1.00 (2) | 4.94 (1) | 4.82 (1) | 8.52 | 1.67 |
| | | | $R_2$ | 4.04 (2) | 6.56 (1) | 1.96 (1) | –1.67 (1) | –1.51 (1) | –2.49 | –4.69 (–1) |
| | | | $R_3$ | –4.72 (1) | –6.92 | –1.41 | 2.73 | 2.31 | 3.58 (–1) | 6.43 (–2) |
| | | | $R_4$ | 2.60 | 3.18 (–1) | 3.90 (–3) | –2.17 (–1) | –1.73 (–1) | –2.53 (–2) | –4.30 (–3) |
| | | | $R_5$ | –5.30 (–2) | –4.32 (–3) | 2.44 (–3) | 6.66 (–3) | 5.11 (–3) | 7.05 (–4) | 1.13 (–4) |
| | | 5000 | $R_0$ | 9.04 (2) | 1.42 (2) | 4.54 (1) | –1.15 (1) | –7.29 | 7.73 (–1) | 1.20 |
| | | | $R_1$ | –5.85 (2) | –8.61 (1) | –2.37 (1) | 1.06 (1) | 6.51 | 1.55 (–1) | –1.57 (–1) |
| | | | $R_2$ | 1.44 (2) | 1.95 (1) | 4.08 | –3.48 | –2.01 | –4.02 (–2) | 5.04 (–2) |
| | | | $R_3$ | –1.68 (1) | –1.98 | –1.73 (–1) | 5.58 (–1) | 3.05 (–1) | 4.89 (–3) | –8.03 (–3) |
| | | | $R_4$ | 9.21 (–1) | 8.41 (–2) | –1.61 (–2) | –4.34 (–2) | –2.27 (–2) | –2.68 (–4) | 6.36 (–4) |
| | | | $R_5$ | –1.86 (–2) | –8.54 (–4) | 1.20 (–3) | 1.32 (–3) | 6.63 (–4) | 4.86 (–6) | –2.00 (–5) |
| | | 10000 | $R_0$ | 9.14 (1) | 1.29 (1) | 3.87 | 1.50 (–1) | 7.18 (–1) | 1.21 | 1.17 |
| | | | $R_1$ | –5.84 (1) | –7.12 | –1.34 | 6.94 (–1) | 2.12 (–1) | –1.71 (–1) | –1.34 (–1) |
| | | | $R_2$ | 1.43 (1) | 1.56 | 1.50 (–1) | –2.22 (–1) | –6.22 (–2) | 5.48 (–2) | 4.31 (–2) |
| | | | $R_3$ | –1.66 | –1.47 (–1) | 1.33 (–2) | 3.44 (–2) | 8.80 (–3) | –8.71 (–3) | –6.87 (–3) |
| | | | $R_4$ | 9.05 (–2) | 5.21 (–3) | –3.32 (–3) | –2.60 (–3) | –5.97 (–4) | 6.87 (–4) | 5.44 (–4) |
| | | | $R_5$ | –1.80 (–3) | –7.71 (–6) | 1.55 (–4) | 7.64 (–5) | 1.54 (–5) | –2.16 (–5) | –1.71 (–5) |

to be continued

Continued from Table 4

$E_{total}/E_e = R_0 + R_1 \times \log(n) + R_2 \times \log^2(n) + R_3 \times \log^3(n) + R_4 \times \log^4(n) + R_5 \times \log^5(n)$

| Particles | $T_n$ (K) | $T_e$ (K) | Parameters | $n_e$ (cm$^{-3}$) | | | | | | |
|---|---|---|---|---|---|---|---|---|---|---|
| | | | | $10^3$ | $5\times10^3$ | $10^4$ | $5\times10^4$ | $10^5$ | $5\times10^5$ | $10^6$ |
| O I | 10000 | 10000 | $R_0$ | 6.64 (4) | 1.34 (4) | 6.70 (3) | 1.30 (3) | 6.17 (2) | 7.47 (1) | 1.66 (1) |
| | | | $R_1$ | –4.92 (4) | –9.89 (3) | –4.95 (3) | –9.60 (2) | –4.54 (2) | –5.28 (1) | –1.02 (1) |
| | | | $R_2$ | 1.43 (4) | 2.88 (3) | 1.44 (3) | 2.79 (2) | 1.31 (2) | 1.47 (1) | 2.46 |
| | | | $R_3$ | –2.04 (3) | –4.10 (2) | –2.05 (2) | –3.95 (1) | –1.85 (1) | –1.98 | –2.57 (–1) |
| | | | $R_4$ | 1.42 (2) | 2.85 (1) | 1.42 (1) | 2.73 | 1.27 | 1.26 (–1) | 9.05 (–3) |
| | | | $R_5$ | –3.80 | –7.63 (–1) | –3.81 (–1) | –7.27 (–2) | –3.36 (–2) | –2.94 (–3) | 9.44 (–5) |
| | | 15000 | $R_0$ | 2.52 (4) | 5.00 (3) | 2.48 (3) | 4.54 (2) | 2.01 (2) | 1.22 (1) | –6.04 (–1) |
| | | | $R_1$ | –1.86 (4) | –3.70 (3) | –1.83 (3) | –3.34 (2) | –1.47 (2) | –7.86 | 1.26 |
| | | | $R_2$ | 5.43 (3) | 1.08 (3) | 5.33 (2) | 9.68 (1) | 4.25 (1) | 2.12 | –4.01 (–1) |
| | | | $R_3$ | –7.73 (2) | –1.53 (2) | –7.59 (1) | –1.37 (1) | –5.99 | –2.71 (–1) | 6.46 (–2) |
| | | | $R_4$ | 5.37 (1) | 1.06 (1) | 5.26 | 9.47 (–1) | 4.09 (–1) | 1.58 (–2) | –5.27 (–3) |
| | | | $R_5$ | –1.44 | –2.85 (–1) | –1.41 (–1) | –2.51 (–2) | –1.08 (–2) | –3.05 (–4) | 1.74 (–4) |
| | | 20000 | $R_0$ | 1.46 (4) | 2.83 (3) | 1.39 (3) | 2.37 (2) | 9.44 (1) | –5.54 | –9.05 |
| | | | $R_1$ | –1.08 (4) | –2.10 (3) | –1.03 (3) | –1.74 (2) | –6.87 (1) | 4.74 | 7.00 |
| | | | $R_2$ | 3.14 (3) | 6.10 (2) | 2.99 (2) | 5.05 (1) | 1.98 (1) | –1.37 | –1.91 |
| | | | $R_3$ | –4.47 (2) | –8.69 (1) | –4.26 (1) | –7.15 | –2.79 | 1.99 (–1) | 2.55 (–1) |
| | | | $R_4$ | 3.10 (1) | 6.03 | 2.95 | 4.92 (–1) | 1.90 (–1) | –1.44 (–2) | –1.65 (–2) |
| | | | $R_5$ | –8.33 (–1) | –1.62 (–1) | –7.91 (–2) | –1.30 (–2) | –4.94 (–3) | 4.22 (–4) | 4.09 (–4) |
| N II | 1000 | 1000 | $R_0$ | –1.95 (3) | –6.81 (2) | –5.22 (2) | –2.69 (2) | –1.58 (2) | –1.12 | 1.19 (1) |
| | | | $R_1$ | 1.46 (3) | 5.13 (2) | 3.93 (2) | 2.00 (2) | 1.16 (2) | 9.76 (–2) | –8.91 |
| | | | $R_2$ | –4.29 (2) | –1.52 (2) | –1.16 (2) | –5.84 (1) | –3.35 (1) | 4.71 (–1) | 2.88 |
| | | | $R_3$ | 6.23 (1) | 2.21 (1) | 1.69 (1) | 8.36 | 4.72 | –1.51 (–1) | –4.60 (–1) |
| | | | $R_4$ | –4.44 | –1.58 | –1.20 | –5.87 (–1) | –3.25 (–1) | 1.73 (–2) | 3.62 (–2) |
| | | | $R_5$ | 1.24 (–1) | 4.42 (–2) | 3.37 (–2) | 1.62 (–2) | 8.79 (–3) | –6.88 (–4) | –1.12 (–3) |
| | | 3000 | $R_0$ | –3.12 (2) | –9.39 (1) | –4.50 (1) | –1.83 | 9.60 (–1) | 1.04 | 9.87 (–1) |
| | | | $R_1$ | 2.36 (2) | 7.08 (1) | 3.41 (1) | 1.97 | –3.01 (–2) | –3.33 (–2) | 9.67 (–3) |
| | | | $R_2$ | –6.98 (1) | –2.08 (1) | –9.92 | –5.32 (–1) | 2.90 (–2) | 1.02 (–2) | –2.86 (–3) |
| | | | $R_3$ | 1.02 (1) | 3.00 | 1.42 | 6.92 (–2) | –7.52 (–3) | –1.56 (–3) | 4.15 (–4) |
| | | | $R_4$ | –7.42 (–1) | –2.12 (–1) | –9.39 (–2) | –4.30 (–3) | 8.02 (–4) | 1.17 (–4) | –2.96 (–5) |
| | | | $R_5$ | 2.03 (–2) | 5.89 (–3) | 2.73 (–3) | 1.01 (–4) | –3.06 (–5) | –3.46 (–6) | 8.21 (–7) |
| | | 5000 | $R_0$ | –2.06 (1) | –2.39 | –5.40 (–2) | 1.01 | 1.00 | 9.98 (–1) | 1.00 |
| | | | $R_1$ | 1.62 (1) | 2.50 | 7.64 (–1) | –1.22 (–2) | –2.62 (–3) | 1.79 (–3) | 8.69 (–5) |
| | | | $R_2$ | –4.78 | –7.26 (–1) | –2.17 (–1) | 4.32 (–3) | 8.28 (–4) | –5.25 (–4) | –1.05 (–5) |
| | | | $R_3$ | 6.94 (–1) | 1.03 (–1) | 3.02 (–2) | –7.46 (–4) | –1.30 (–4) | 7.58 (–5) | –1.25 (–6) |
| | | | $R_4$ | –4.93 (–2) | –7.19 (–3) | –2.05 (–3) | 6.28 (–5) | 1.00 (–5) | –5.34 (–6) | 3.45 (–7) |
| | | | $R_5$ | 1.38 (–3) | 1.96 (–4) | 5.41 (–5) | –2.06 (–6) | –3.05 (–7) | 1.46 (–7) | –1.91 (–8) |

to be continued

Continued from Table 4

$E_{total}/E_e = R_0 + R_1 \times \log(n) + R_2 \times \log^2(n) + R_3 \times \log^3(n) + R_4 \times \log^4(n) + R_5 \times \log^5(n)$

| Particles | $T_n$ (K) | $T_e$ (K) | Parameters | $n_e$ (cm$^{-3}$) | | | | | | |
|---|---|---|---|---|---|---|---|---|---|---|
| | | | | $10^3$ | $5\times10^3$ | $10^4$ | $5\times10^4$ | $10^5$ | $5\times10^5$ | $10^6$ |
| N II | 3000 | 3000 | $R_0$ | –1.11 (3) | –3.19 (2) | –1.80 (2) | –3.96 (1) | –1.76 (1) | –8.27 (–1) | 4.77 (–1) |
| | | | $R_1$ | 8.91 (2) | 2.56 (2) | 1.44 (2) | 3.19 (1) | 1.45 (1) | 1.42 | 4.08 (–1) |
| | | | $R_2$ | –2.83 (2) | –8.11 (1) | –4.56 (1) | –9.94 | –4.51 | –4.41 (–1) | –1.27 (–1) |
| | | | $R_3$ | 4.46 (1) | 1.28 (1) | 7.15 | 1.54 | 6.97 (–1) | 6.80 (–2) | 1.96 (–2) |
| | | | $R_4$ | –3.49 | –9.96 (–1) | –5.56 (–1) | –1.18 (–1) | –5.34 (–2) | –5.21 (–3) | –1.50 (–3) |
| | | | $R_5$ | 1.08 (–1) | 3.08 (–2) | 1.72 (–2) | 3.62 (–3) | 1.63 (–3) | 1.59 (–4) | 4.61 (–5) |
| | | 5000 | $R_0$ | –6.67 (1) | –8.73 | –9.80 (–1) | 5.02 | 5.05 | 3.06 | 2.24 |
| | | | $R_1$ | 5.42 (1) | 7.77 | 1.58 | –3.16 | –3.19 | –1.62 | –9.69 (–1) |
| | | | $R_2$ | –1.72 (1) | –2.46 | –4.99 (–1) | 9.90 (–1) | 9.96 (–1) | 5.05 (–1) | 3.02 (–1) |
| | | | $R_3$ | 2.72 | 3.86 (–1) | 7.78 (–2) | –1.54 (–1) | –1.55 (–1) | –7.84 (–2) | –4.69 (–2) |
| | | | $R_4$ | –2.13 (–1) | –3.00 (–2) | –5.97 (–3) | 1.20 (–2) | 1.20 (–2) | 6.05 (–3) | 3.62 (–3) |
| | | | $R_5$ | 6.60 (–3) | 9.26 (–4) | 1.81 (–4) | –3.69 (–4) | –3.69 (–4) | –1.86 (–4) | –1.11 (–4) |
| | 10000 | 10000 | $R_0$ | –1.01 (4) | –1.88 (3) | –8.48 (2) | –5.00 (1) | 2.43 (1) | 1.33 (1) | –3.94 (–1) |
| | | | $R_1$ | 6.93 (3) | 1.28 (3) | 5.71 (2) | 2.49 (1) | –2.37 (1) | –9.47 | 1.25 |
| | | | $R_2$ | –1.83 (3) | –3.34 (2) | –1.47 (2) | –2.94 | 9.07 | 2.87 | –4.49 (–1) |
| | | | $R_3$ | 2.32 (2) | 4.17 (1) | 1.79 (1) | –2.87 (–1) | –1.66 | –4.27 (–1) | 8.04 (–2) |
| | | | $R_4$ | –1.39 (1) | –2.44 | –1.00 | 7.67 (–2) | 1.45 (–1) | 3.11 (–2) | –7.17 (–3) |
| | | | $R_5$ | 3.12 (–1) | 5.23 (–2) | 2.00 (–2) | –3.83 (–3) | –4.86 (–3) | –8.77 (–4) | 2.56 (–4) |
| | | 15000 | $R_0$ | –3.74 (3) | –6.61 (2) | –2.81 (2) | –1.18 (–1) | –5.85 | –2.25 (1) | –1.08 (1) |
| | | | $R_1$ | 2.57 (3) | 4.50 (2) | 1.89 (2) | 7.20 | 5.17 | 1.82 (1) | 9.02 |
| | | | $R_2$ | –6.80 (2) | –1.18 (2) | –4.86 (1) | –1.34 | –1.55 | –5.59 | –2.72 |
| | | | $R_3$ | 8.61 (1) | 1.47 (1) | 5.89 | 6.92 (–2) | 2.32 (–1) | 8.49 (–1) | 4.07 (–1) |
| | | | $R_4$ | –5.16 | –8.55 (–1) | –3.29 (–1) | 4.73 (–3) | –1.74 (–2) | –6.37 (–2) | –2.99 (–2) |
| | | | $R_5$ | 1.15 (–1) | 1.83 (–2) | 6.53 (–3) | –4.13 (–4) | 5.20 (–4) | 1.88 (–3) | 8.67 (–4) |
| | | 20000 | $R_0$ | –1.92 (3) | –3.25 (2) | –1.30 (2) | –5.97 | –1.03 (1) | –9.79 | –3.49 (–1) |
| | | | $R_1$ | 1.32 (3) | 2.21 (2) | 8.81 (1) | 5.09 | 9.28 | 8.34 | 1.04 |
| | | | $R_2$ | –3.49 (2) | –5.79 (1) | –2.27 (1) | –1.47 | –3.03 | –2.55 | –3.17 (–1) |
| | | | $R_3$ | 4.42 (1) | 7.21 | 2.76 | 2.09 (–1) | 4.89 (–1) | 3.86 (–1) | 4.80 (–2) |
| | | | $R_4$ | –2.65 | –4.21 (–1) | –1.55 (–1) | –1.48 (–2) | –3.90 (–2) | –2.89 (–2) | –3.60 (–3) |
| | | | $R_5$ | 5.93 (–2) | 9.05 (–3) | 3.12 (–3) | 4.21 (–4) | 1.22 (–3) | 8.52 (–4) | 1.07 (–4) |

## Supplementary Materials

### A. Electron-Impact Collisional Excitation Cross Sections Used in this Work

1) O I: Figure S1 (a).

2) C I: Figure S1 (b).

3) N I: Figure S1 (c).

4) O II: Figure S1 (d).

5) C II: Figure S1 (e).

6) N II: Figure S1 (f).

### B. Emission Lines

The following (Figure S2) are the emission rates calculated with $n_e$ of $10^3$ cm$^{-3}$. For each metal species only the most important emission lines are shown. Note also that the relative importance of different lines could change with different $n_e$. Figure 2 in the main text considers different combinations $n_e$ and $T_e$.

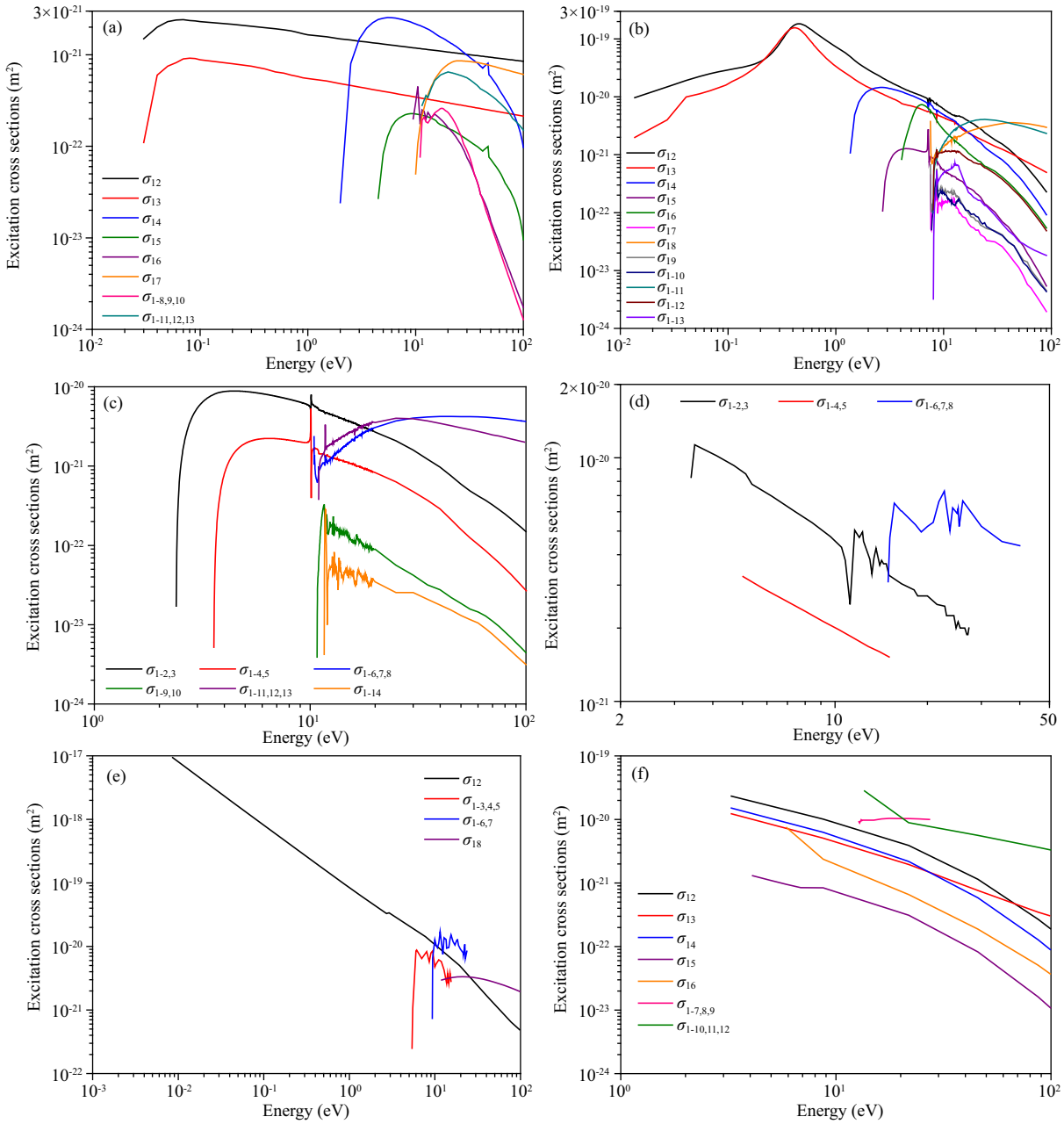


**Figure S1**. (a) Collisional excitation cross sections of O I. $\sigma_{12}$ and $\sigma_{13}$ are from Itikawa et al. (1990). $\sigma_{14}$ and $\sigma_{15}$ are from Morgan database and Henry et al. (1969). $\sigma_{17}$ are from Johnson et al. (2005). $\sigma_{16}$, $\sigma_{1-8,9,10}$ and $\sigma_{1-11,12,13}$ are from Zatsarinny and Tayal (2002). (b) Collisional excitation cross sections of C I. Data are from Wang Y et al. (2013), Morgan database, Zatsarinny and Bartschat (2004), and Allan et al. (2006). (c) Collisional excitation cross sections of N I. Data are from Wang Y et al. (2014), Morgan database, Zatsarinny and Bartschat (2004), and Allan et al. (2006). (d) Collisional excitation cross sections of O II. $\sigma_{1-2,3}$ and $\sigma_{1-6,7,8}$ are from Zuo M et al. (1995). $\sigma_{1-4,5}$ are from Henry et al. (1969). (e) Collisional excitation cross sections of C II. $\sigma_{12}$ are from Zhang HL and Sampson (1994) and Tambe (1977). $\sigma_{1-3,4,5}$ and $\sigma_{1-6,7}$ are from Smith et al. (1996). $\sigma_{18}$ are from Suno and Kato (2006). (f) Collisional excitation cross sections of N II. $\sigma_{12}$, $\sigma_{13}$, $\sigma_{14}$, $\sigma_{15}$, $\sigma_{16}$, and $\sigma_{1-10,11,12}$ are from Zhang HL and Sampson (1996). $\sigma_{1-7,8,9}$ are from Ormonde et al. (1973).

### C. Model Validation

Figure S3 shows the typical profiles of electron temperature ($T_e$), neutral temperature ($T_n$), electron density ($n_e$), and O I density (the most abundant atomic species) in modern Earth's thermosphere under solar maximum conditions (Tian F et al., 2008b). These data are used as inputs in the population balance model to calculate the O I emission rates as a function of altitude.

### D. Atomic Collisions Energy Transfer

The momentum and energy equations describing an inelastic collision is:

$$m_1 v_1 + m_2 v_2 = m_1 v_1' + m_2 v_2', \tag{S1}$$

$$\frac{1}{2} m_1 {v_1}^2 + \frac{1}{2} m_2 {v_2}^2 = \frac{1}{2} m_1 {v_1}'^2 + \frac{1}{2} m_2 {v_2}'^2 + \Delta E. \tag{S2}$$

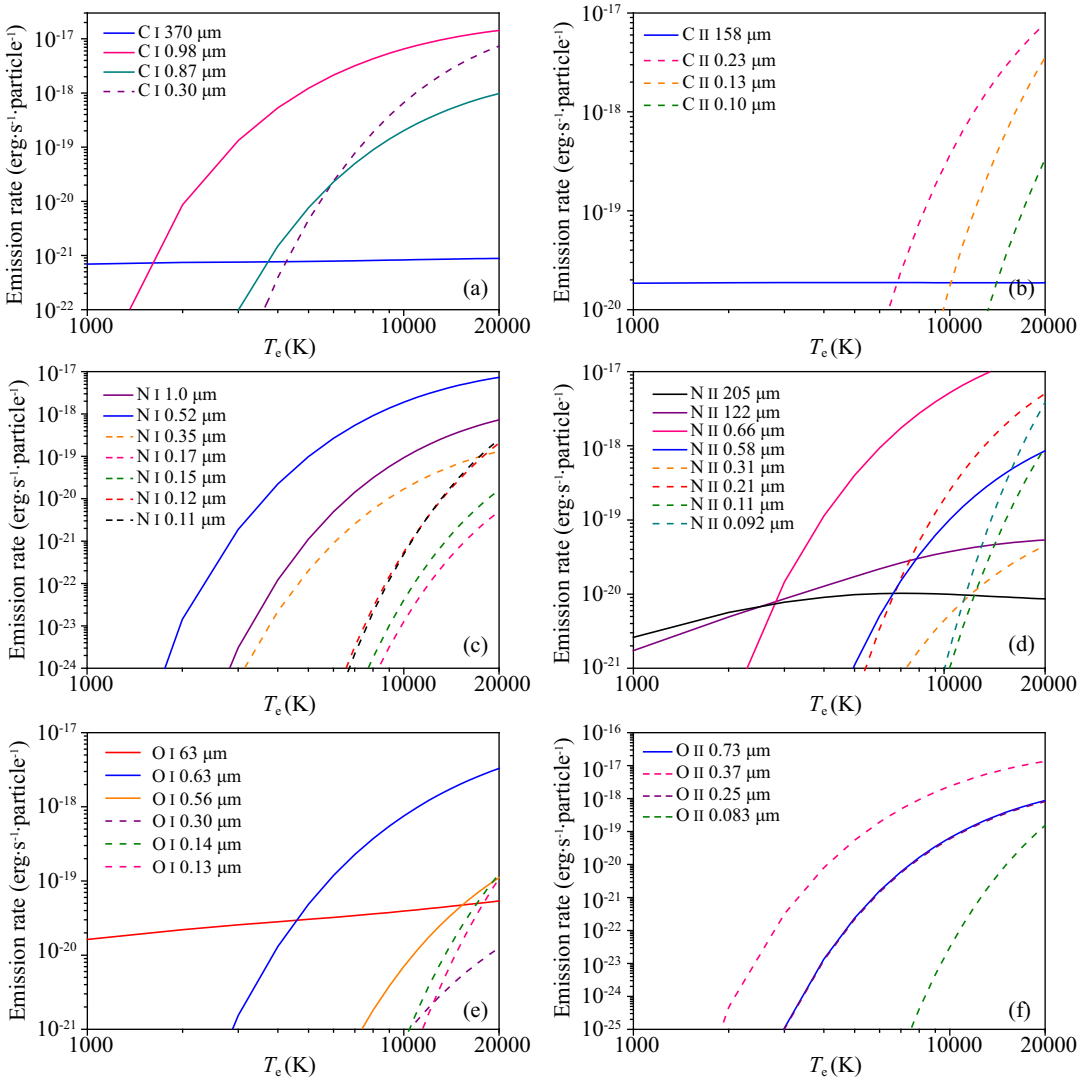


**Figure S2**. Electron-collision-induced emission rates of C, N, and O and their ions for $n_e$=10$^3$ cm$^{-3}$. For each metal species only the most important emission lines are shown. The relative importance of different lines could change with different $n_e$.

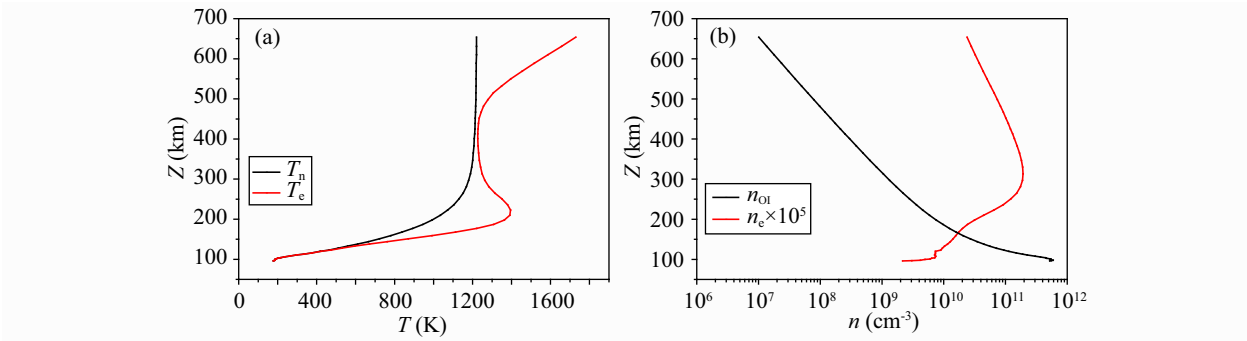


**Figure S3**. Temperature (panel a) and density (panel b) profiles of modern Earth in solar maximum conditions (Tian F et al., 2008b). The black and red curves represent electron and neutral temperatures respectively in panel a, and represent the densities of electrons (multiplied by 10$^5$) and O I in panel b respectively.

The equations can be modified to the following:

$$m_1(v_1 - v_1') = m_1\Delta v_1 = -m_2\Delta v_2, \tag{S3}$$

$$m_1\Delta v_1(v_1 + v_1') = -m_2\Delta v_2(v_2 + v_2') + 2\Delta E. \tag{S4}$$

Merging equation (S3) with (S4):

$$m_1\Delta v_1(v_1+v_1{}') = m_1\Delta v_1(v_2+v_2{}') + 2\Delta E$$
$$= m_1\Delta v_1\left(2v_2+\frac{m_1}{m_2}\Delta v_1\right)+2\Delta E,$$

which is equivalent to

$$\Delta E = \frac{1}{2}m_1\Delta v_1(v_1+v_1{}'-2v_2) - \frac{1}{2}\frac{m_1{}^2}{m_2}\Delta v_1{}^2.$$

If $m_1 = m_2 = m$,

$$\Delta E = \frac{1}{2}m\Delta v_1(v_1+v_1{}'-2v_2) - \frac{1}{2}m\Delta v_1{}^2 = m\Delta v_1(v_1{}'-v_2).$$

When the target does not gain much kinetic energy, the excitation could gain maximum energy. In this case $v_2 \ll v_1'$,

$$\Delta E = m(v_1 - v_1{}')v_1{}'.$$

To obtain maximum $\Delta E$ requires

$$\frac{\mathrm{d}\Delta E}{\mathrm{d}v_1{}'} = v_1 - 2v_1{}' = 0,$$

which is reached when

$$v_1{}' = \frac{1}{2}v_1.$$

Thus the maximum $\Delta E$ is: $\Delta E_{\max} = \frac{1}{4}mv_1{}^2$ or half the initial kinetic energy of the impactor.

We also note that this derivation is for 1D case. For 3D case the transfer of kinetic energy to internal energy could be less efficient.

## Acknowledgements

We thank the anonymous reviewers for their constructive suggestions and comments, which helped to improve the quality of the paper. F. Tian thanks discussions with P. Judge and R. Wordsworth during the preparation of this work. L. Liu and F. Tian are supported by the National Natural Science Foundation of China (11661161014) and Tsinghua University Initiative Science Research Program (523001028).

## References

Airapetian, V. S., Glocer, A., Khazanov, G. V., Loyd, R. O. P., France, K., Sojka, J., Danchi, W. C., and Liemohn, M. W. (2017). How hospitable are space weather affected habitable zones? The role of ion escape. *Astrophys. J. Lett.*, *836*(1), L3. https://doi.org/10.3847/2041-8213/836/1/L3

Allan, M., Zatsarinny, O., and Bartschat, K. (2006). Near-threshold absolute angle-differential cross sections for electron-impact excitation of argon and xenon. *Phys. Rev. A*, *74*(3), 030701. https://doi.org/10.1103/PhysRevA.74.030701

Black, J. H. (1981). The physical state of primordial intergalactic clouds. *Mon. Not. R. Astron. Soc.*, *197*(3), 553–563. https://doi.org/10.1093/mnras/197.3.553

Charbonneau, D., Brown, T. M., Noyes, R. W., and Gilliland, R. L. (2002). Detection of an extrasolar planet atmosphere. *Astrophys. J.*, *568*(1), 377–384. https://doi.org/10.1086/338770

Glover, S. C. O., and Jappsen, A. K. (2008). Star formation at very low metallicity. I. Chemistry and cooling at low densities. *Astrophys. J.*, *666*(1), 1–19. https://doi.org/10.1086/519445

Henry, R. J. W., Burke, P. G., and Sinfailam, A. L. (1969). Scattering of electrons by C, N, O, $N^+$, $O^+$, and $O^{++}$. *Phys. Rev.*, *178*(1), 218–225. https://doi.org/10.1103/PhysRev.178.218

Itikawa, Y., Hayashi, M., Ichimura, A., Onda, K., Sakimoto, K., Takayanagi, K., Nakamura, M., Nishimura, H., and Takayanagi, T. (1990). Cross sections for collisions of electrons and photons with atomic oxygen. *J. Phys. Chem. Ref. Data*, *19*(3), 637–651. https://doi.org/10.1063/1.555762

Johnson, P. V., McConkey, J. W., Tayal, S. S., and Kanik, I. (2005). Collisions of electrons with atomic oxygen: current status. *Can. J. Phys.*, *83*(6), 589–616. https://doi.org/10.1139/p05-034

Kockarts, G., and Peetermans, W. (1970). Atomic oxygen infrared emission in the earth's upper atmosphere. *Planet. Space Sci.*, *18*(2), 271–285. https://doi.org/10.1016/0032-0633(70)90163-7

Koskinen, T. T., Harris, M. J., Yelle, R. V., and Lavvas, P. (2013a). The escape of heavy atoms from the ionosphere of HD209458b. I. A photochemical-dynamical model of the thermosphere. *Icarus*, *226*(2), 1678–1694. https://doi.org/10.1016/j.icarus.2012.09.027

Koskinen, T. T., Yelle, R. V., Harris, M. J., and Lavvas, P. (2013b). The escape of heavy atoms from the ionosphere of HD209458b. II. Interpretation of the observations. *Icarus*, *226*(2), 1695–1708. https://doi.org/10.1016/j.icarus.2012.09.026

Linsky, J. L., Hao, Y., France, K., Froning, C. S., Green, J. C., Stocke, J. T., and Osterman, S. N. (2010). Observations of mass loss from the transiting exoplanet HD 209458b. *Astrophys. J.*, *717*(2), 1291–1299. https://doi.org/10.1088/0004-637X/717/2/1291

Lopez, E. D., Fortney, J. J., and Miller, N. (2012). How thermal evolution and mass-loss sculpt populations of super-Earths and sub-Neptunes: application to the Kepler-11 system and beyond. *Astrophys. J.*, *761*(1), 59. https://doi.org/10.1088/0004-637X/761/1/59

Luger, R., Barnes, R., Lopez, E., Fortney, J., Jackson, B., and Meadows, V. (2015). Habitable evaporated cores: transforming mini-Neptunes into super-Earths in the habitable zones of M dwarfs. *Astrobiology*, *15*(1), 57–88. https://doi.org/10.1089/ast.2014.1215

Massol, H., Hamano, K., Tian, F., Ikoma, M., Abe, Y., Chassefière, E., Davaille, A., Genda, H., Güdel, M., … Lammer, H. (2016). Formation and evolution of protoatmospheres. *Space Sci. Rev.*, *205*(1-4), 153–211. https://doi.org/10.1007/s11214-016-0280-1

Morgan database, www.lxcat.net, retrieved on December 26, 2016.

Murray-Clay, R. A., Chiang, E. I., and Murray, N. (2009). Atmospheric escape from hot Jupiters. *Astrophys. J.*, *693*(1), 23–42. https://doi.org/10.1088/0004-637X/693/1/23

Ormonde, S., Smith, K., Torres, B. W., and Davies, A. R. (1973). Configuration-interaction effects in the scattering of electrons by atoms and ions of nitrogen and oxygen. *Phys. Rev. A*, *8*(1), 262–295. https://doi.org/10.1103/PhysRevA.8.262

Owen, J. E., and Jackson, A. P. (2012). Planetary evaporation by UV and X-ray radiation: basic hydrodynamics. *Mon. Not. R. Astron. Soc.*, *425*(4), 2931–2947. https://doi.org/10.1111/j.1365-2966.2012.21481.x

Roble, R. G., Ridley, E. C., and Dickinson, R. E. (1987). On the global mean structure of the thermosphere. *J. Geophys. Res.*, *92*(A8), 8745–8758. https://doi.org/10.1029/JA092iA08p08745

Roble, R. G. (1995). Major greenhouse cooling (yes, cooling): The upper atmosphere response to increased $CO_2$. *Rev. Geophys.*, *33*(S1), 539–546. https://doi.org/10.1029/95RG00118

Schaefer, L., Wordsworth, R. D., Berta-Thompson, Z., and Sasselov, D. (2016). Predictions of the atmospheric composition of GJ 1132b. *Astrophys. J.*, *829*(2), 63. https://doi.org/10.3847/0004-637X/829/2/63

Seaton, M. J. (1959). Radiative recombination of hydrogenic ions. *Mon. Not. R. Astron. Soc.*, *119*(2), 81–89. https://doi.org/10.1093/mnras/119.2.81

Shaikhislamov, I. F., Khodachenko, M. L., Sasunov, Y. L., Lammer, H., Kislyakova, K. G., and Erkaev, N. V. (2014). Atmosphere expansion and mass loss of close-orbit giant exoplanets heated by stellar XUV. I. Modeling of hydrodynamic escape of upper atmospheric material. *Astrophys. J.*, *795*(2), 132. https://doi.org/10.1088/0004-637X/795/2/132

Shematovich, V. I., Ionov, D. E., and Lammer, H. (2014). Heating efficiency in hydrogen-dominated upper atmospheres. *Astron. Astrophys.*, *571*, A94.

https://doi.org/10.1051/0004-6361/201423573

Shuker, R., Gallagher, A., and Phelps, A. V. (1980). Models of high-power discharges for metal-Xe excimer lasers. *J. Appl. Phys.*, *51*(3), 1306–1320. https://doi.org/10.1063/1.327825

Sing, D. K., Lecavelier, A., Désert, J. M., Vidal-Madjar, A., and Ballester, G. (2008a). Absorption spectra of the prototype hot-Jupiters: determination of atmospheric constituents and structure. *Proc. Int. Astron. Union*, *4*(S253), 532–535. https://doi.org/10.1017/S1743921308027130

Sing, D. K., Vidal-Madjar, A., Des Etangs, A. L., Désert, J. M., Ballester, G., and Ehrenreich, D. (2008b). Determining atmospheric conditions at the terminator of the hot Jupiter HD 209458b. *Astrophys. J.*, *686*(1), 667–673. https://doi.org/10.1086/590076

Sing, D. K., Désert, J. M., Fortney, J. J., Des Etangs, A. L., Ballester, G. E., Cepa, J., Ehrenreich, D., López-Morales, M., Pont, F., … Vidal-Madjar, A. (2011). Gran telescopio canarias OSIRIS transiting exoplanet atmospheric survey: Detection of potassium in XO-2b from narrowband spectrophotometry. *Astron. Astrophys.*, *527*(9), A73. https://doi.org/10.1051/0004-6361/201015579

Smith, S. J., Zuo, M., Chutjian, A., Tayal, S. S., and Williams, I. D. (1996). Electron excitation cross sections for the C II transitions $2s^22p\ ^2P^O$ $2s2p^2\ ^4P$, $^2D$, and $^2S$. *Astrophys. J.*, *463*, 808. https://doi.org/10.1086/177292

Suno, H., and Kato, T. (2006). Cross section database for carbon atoms and ions: Electron-impact ionization, excitation, and charge exchange in collisions with hydrogen atoms. *At. Data Nucl. Data Tables*, *92*(4), 407–455. https://doi.org/10.1016/j.adt.2006.01.001

Tambe, B. R. (1977). Electron-impact-induced fine-structure transitions in singly ionized carbon. *J. Phys. B Atomic Mol. Phys.*, *10*(7), L249–L252. https://doi.org/10.1088/0022-3700/10/7/004

Tian, F., Toon, O. B., Pavlov, A. A., and De Sterck, H. (2005). Transonic hydrodynamic escape of hydrogen from extrasolar planetary atmospheres. *Astrophys. J.*, *621*(2), 1049–1060. https://doi.org/10.1086/427204

Tian, F., Kasting, J. F., Liu, H. L., and Roble, R. G. (2008a). Hydrodynamic planetary thermosphere model. 1. Response of the Earth's thermosphere to extreme solar EUV conditions and the significance of adiabatic cooling. *J. Geophys. Res.*, *113*(E5), E05008. https://doi.org/10.1029/2007JE002946

Tian, F., Solomon, S. C., Qian, L. Y., Lei, J. H., and Roble, R. G. (2008b). Hydrodynamic planetary thermosphere model: 2. Coupling of an electron transport/energy deposition model. *J. Geophys. Res.*, *113*(E7), E07005. https://doi.org/10.1029/2007JE003043

Tian, F. (2009). Thermal escape from super earth atmospheres in the habitable zones of M stars. *Astrophys. J.*, *703*(1), 905–909. https://doi.org/10.1088/0004-637X/703/1/905

Tian, F., Kasting, J. F., and Solomon, S. C. (2009). Thermal escape of carbon from the early Martian atmosphere. *Geophys. Res. Lett.*, *36*(2), L02205. https://doi.org/10.1029/2008GL036513

Tian, F. (2015). Atmospheric escape from solar system terrestrial planets and exoplanets. *Annu. Rev. Earth Planet. Sci.*, *43*, 459–476. https://doi.org/10.1146/annurev-earth-060313-05483

Vidal-Madjar A., Désert, J. M., Des Etangs, A. L., Hébrard, G., Ballester, G. E., Ehrenreich, D., Ferlet, R., McConnell, J. C., Mayor, M., and Parkinson, C. D. (2004). Detection of oxygen and carbon in the hydrodynamically escaping atmosphere of the extrasolar planet HD 209458b. *Astrophys. J.*, *604*(1), L69–L72. https://doi.org/10.1086/383347

Wang, Y., Zatsarinny, O., and Bartschat, K. (2013). B-spline R-matrix-with-pseudostates calculations for electron-impact excitation and ionization of carbon. *Phys. Rev. A*, *87*(1), 012704. https://doi.org/10.1103/PhysRevA.87.012704

Wang, Y., Zatsarinny, O., and Bartschat, K. (2014). B-spline R-matrix-with-pseudostates calculations for electron-impact excitation and ionization of nitrogen. *Phys. Rev. A*, *89*(6), 062714. https://doi.org/10.1103/PhysRevA.89.062714

Yelle, R. V. (2004). Aeronomy of extra-solar giant planets at small orbital distances. *Icarus*, *170*(1), 167–179. https://doi.org/10.1016/j.icarus.2004.02.008

Zatsarinny, O., and Tayal, S. S. (2002). *R*-matrix calculation with non-orthogonal orbitals for electron-impact excitation of atomic oxygen. *J. Phys. B At. Mol. Opt. Phys.*, *35*(2), 241–253. https://doi.org/10.1088/0953-4075/35/2/304

Zatsarinny, O., and Bartschat, K. (2004). *B*-spline Breit-Pauli *R*-matrix calculations for electron collisions with argon atoms. *J. Phys. B At. Mol. Opt. Phys.*, *37*(23), 4693–4706. https://doi.org/10.1088/0953-4075/37/23/010

Zhang, H. L., and Sampson, D. H. (1994). Relativistic distorted-wave collision strengths and oscillator strengths for the 105 $\Delta n$=0 transitions with $n$=2 in the 85 B-like ions with $8 \leq Z \leq 92$. *At. Data Nucl. Data Tables*, *56*(1), 41–104. https://doi.org/10.1006/adnd.1994.1002

Zhang, H. L., and Sampson, D. H. (1996). Relativistic distorted-wave collision strengths and oscillator strengths for the $\Delta n$=0 transitions with $n$=2 in C-Like Ions with $9 \leq Z \leq 54$. *At. Data Nucl. Data Tables*, *63*(2), 275–314. https://doi.org/10.1006/adnd.1996.0014

Zuo, M., Smith, S. J., Chutjian, A., Williams, I. D., Tayal, S. S., and Mclaughlin, B. M. (1995). Electron excitation cross sections for the $2s^22p^3\ ^4S^o \rightarrow 2s^22p^3\ ^2D^o$ (forbidden) and $^4S^o \rightarrow 2s2p^4\ ^4P$ (resonance) transitions in O II. *Astrophys. J.*, *440*(1), 421–429. https://doi.org/10.1086/175284